ANALYSIS OF TEC VARIATION DURING JUNE 21, 2020 ANNULAR SOLAR ECLIPSE OVER ADDIS ABABA AND DJIBOUTI

By

Shibre Sete

A THESIS SUBMITTED IN PARTIAL FULFILLMENT OF THE
REQUIREMENTS FOR THE DEGREE OF
MASTER OF SCIENCE IN SPACE PHYSICS
AT
ADDIS ABABA UNIVERSITY
SCHOOL OF GRADUATE STUDIES
ADDIS ABABA, ETHIOPIA

OCTOBER, 2021

© Shibre Sete, 2021

ADDIS ABABA UNIVERSITY

SCHOOL OF GRADUATE STUDIES

DEPARTMENT OF PHYSICS

The undersigned hereby certify that they have read and recommend to the school of graduate studies for acceptance a thesis entitled **"ANALYSIS OF TEC VARIATION DURING JUNE 21, 2020 ANNULAR SOLAR ECLIPSE OVER ADDIS ABABA AND DJIBOUTI"** by **Shibre Sete** in partial fulfillment of the requirements for the degree of **Master of Science in**

Space Physics.

Dated: *October*, 2021

Approved by the Examination Committee:

1. Advisor: Dr. Yitagesu Elfagd _____
2. Examiner: Dr. Girum Abebe _____
3. Examiner: Dr. Gemechu Fanta _____
4. Chairwoman: Dr. Newayemedhin Aberra _____

ADDIS ABABA UNIVERSITY

Date: **October, 2021**

Author: **Shibre Sete**

Title: **ANALYSIS OF TEC VARIATION DURING JUNE 21, 2020 ANNULAR SOLAR ECLIPSE OVER ADDIS ABABA AND DJIBOUTI**

Department: **Physics**

Degree: **M.Sc** Convocation: **October** Year: **2021**

Permission is herewith granted to Addis Ababa University to circulate and to have copied for non-commercial purposes, at its discretion, the above title upon the request of individuals or institutions.

_____

Signature of Author

THE AUTHOR RESERVES OTHER PUBLICATION RIGHTS, AND NEITHER THE THESIS NOR EXTENSIVE EXTRACTS FROM IT MAY BE PRINTED OR OTHERWISE REPRODUCED WITHOUT THE AUTHOR'S WRITTEN PERMISSION.

THE AUTHOR ATTESTS THAT PERMISSION HAS BEEN OBTAINED FOR THE USE OF ANY COPYRIGHTED MATERIAL APPEARING IN THIS THESIS (OTHER THAN BRIEF EXCERPTS REQUIRING ONLY PROPER ACKNOWLEDGMENT IN SCHOLARLY WRITING) AND THAT ALL SUCH USE IS CLEARLY ACKNOWLEDGED.

Contents

Acknowledgments

I would like to express my gratitude to everyone who helped me finish this thesis, even though I could not list their names because they are so many of them. First and foremost, I'd like to convey my gratefulness to my advisor Dr. Yitagesu Elfagd, for being there for me whenever I needed help, for his kindness and guidance. This paper would not have been completed without his assistance and active participation in every step of the process.

My gratitude extends to the Physics Department for letting me start my M.Sc and the Addis Ababa University for sponsoring me. I would like to thank, my colleagues, teachers, for encouraging me from day one. A special thanks goes to Dr. Teshome Senbeta, Chairman of the Physics Department, for initiating me to start my M.Sc. Semahegn Abayneh, for the MATLAB installation and for all the technical advice. Dr. Tilahun Tesfaye, for the registration process. Thank you very much you all. Tsilat Adinew, in particular, is deserving of special praise. She was very much of a mother for me, I would like to express my appreciation for all of her help during my studies.

I would like to express my gratitude to Alemayehu Mengesha, Assistant Professor of Space Physics (From IGSSA), Dr. Tsegaye Kassa, Associate Professor of Space Physics (From Bahir Dar University), for their every help and encouragement. I wanted to thank you for your patience to answer my every single questions.

I very much wanted to thank Dr. Tadesse Terefe (From IGSSA), Dr. Girum Abebe (From IGSSA) and Dr. Gemechu Fanta (From ESSTI), for their constructive, encouraging comments and for taking the time to suggest ways to enhance our work.

I want to thank my families, for being there for me, for their patience and for loving me no matter what. My friends, I wanted to thank you for all the shared fun, for your everyday 'how is it going?' question. Classmates, I thank you for everything we had together, it means a lot.

Abstract

On June 21, 2020, an annular solar eclipse happened. The annular eclipse's central path passed through parts of Central and Eastern Africa. A partial solar eclipse was visible across much of Africa and it traverses Ethiopia and Djibouti. During a solar eclipse the Moon blocks a portion of the solar radiation from reaching the Earth. Following the eclipse a decrease in the ionization is expected due to the obscuration of solar radiation, and thus a decrease in the amount of ionospheric total electron content (TEC). The effect of this partial solar eclipse on the ionospheric TEC was studied using two Global Positioning System (GPS) stations found in Addis Ababa and Djibouti. The objective of this thesis is to study the effect of the June 21, 2020 annular eclipse on the ionospheric TEC. Because eclipse geometry varies from eclipse to eclipse, it's not always clear whether a difference in ionospheric reaction is due to a change in eclipse time of occurrence, obscuration level, geometry, or background conditions such as: different solar and geomagnetic activities, seasons, latitudes and longitudes. Therefore, individual eclipse studies are significant. TEC data taken from the two GPS stations were used to examine the ionospheric behavior during the eclipse. The partial solar eclipse was observed to cause a significant TEC depletion during the eclipse period at both stations. Which indicates that the amount of TEC in the ionosphere was affected by the decrease in solar radiation during the eclipse. The TEC measurements during the eclipse period were compared to two days before, two days after the eclipse period and three years of June 21 to make sure that the cause of the TEC depletion was not due to a daily variation in the ionosphere. A maximum TEC reduction of up to 35% were observed compared to the days after and before the eclipse. A time lag of 45 and 15 minutes were found between the maximum obscuration and a maximum TEC depletion over ADIS and DJIG, respectively. After the eclipse ended, the TEC began to return to normal levels and recovered fully after 1 hr over DJIG and 1 hr and 18 minutes over ADIS stations. The TEC reduction shows the partial solar

eclipse affects the ionospheric TEC and since the ionosphere is mostly governed by the photoionization, the decrease in solar radiation causes the density of the ionosphere to decrease. The eclipse occurred during a period of low solar and magnetic activity. The reference days TEC data and the magnetic activity indicated the eclipse was the cause of the TEC depletion. Further research is needed to study the effect of the eclipse in the low latitude region as it can be affected by the equatorial ionization anomaly.
Keywords: Solar Eclipse; Total Electron Content; Ionosphere; Equatorial Ionization Anomaly

List of Figures

List of Tables

Chapter 1

Introduction

The ionosphere is the upper layer of the atmosphere, formed when the Sun's energy ionizes the atoms and molecules within it. Solar radiation, is the fundamental cause of this layer's existence. As Global Positioning System (GPS) signals pass through the ionosphere, they are inevitably affected by this zone of unbound electrons and ions. The ionosphere's physical behavior is influenced by a variety of natural and man made events. The solar eclipse is one of these natural phenomena that has an apparent effect on the ionosphere. When the Sun, Earth, and Moon are aligned during the new Moon phase, the Moon is squarely between the Sun and the Earth, and its shadow falls on the Earth, a solar eclipse occurs [1]. The type of eclipse seen from a specific point is determined by whether the Moon passes directly between the Earth and the Sun or merely partially between the Earth and the Sun [2].

Solar eclipses are usually dissimilar, with varying Sun-Moon-Earth alignment geometries and lunar orbital properties, such that; longitude of perigee and longitude of ascending node [3]. There are mainly three types of solar eclipses. A total, an annular and a partial solar eclipse. A total solar eclipse occurs when the Moon's umbral shadow crosses the Earth and the Sun's disk is fully obstructed by the Moon in its maximum phase of eclipse. The Moon, on the other hand, appears to obstruct part of the Sun's disk during the partial eclipse. At the greatest phase of an annular solar eclipse, the Sun appears as a blindingly bright ring surrounding the Moon as the Moon's antumbral shadow traverses the Earth. An annular solar eclipse happens when the Moon's apparent diameter is smaller than the Sun's, covering most of the Sun's light and giving the appearance of an annulus to the Sun. When the Sun and Moon are not completely aligned, a partial eclipse occurs, and the Moon only partially obscures the Sun.

In terms of communication and navigation, the ionosphere is a vital region and studying the ionosphere is very important as it can be affected by a variety of factors that can cause the ionization to be reduced or enhanced. An unusual decrease or increase in the ionospheric ionization can affect the satellites, radio and GPS signals in that region. A solar eclipse's effects are always unique, as it can occur under a variety of solar activity and geomagnetic conditions, at various geographic latitudes and longitudes, and during varying seasons and local times of day. Eclipses offer a once in a lifetime opportunity to investigate the ionospheric and atmospheric impacts of the obscuration created by the Moon's quickly shifting shadow across the Earth. Because of the various Sun-Earth-Moon alignment geometries and lunar orbital features, eclipses do not reoccur in any predictable pattern. As a result, individual eclipse studies are required [4]. It's not always possible to tell if a difference in the ionospheric reaction is due to a change in eclipse onset time, obscuration level, geometry, or background conditions such as: solar and geomagnetic activities, latitude and longitudes, seasons and local times [5]. Therefore, it is important to study the ionosphere during every eclipses over every places that witnessed an eclipse.

On June 21, 2020, between 03:51 and 09:30 Universal Time (UT), an annular solar eclipse crossed the low latitude ionosphere from Africa to Southeast Asia, with a unique trajectory where the maximum geographic latitude of the totality was around 30°N [6]. The annular eclipse's central path passed through parts of Central and Eastern Africa, the southern Arabian Peninsula, parts of South Asia and the Himalayas. The eclipse was partial over Addis Ababa and Djibouti regions, with a magnitude of 0.9187 and 0.9209, respectively. Which are the regions of interest for this study. They are found in the East African low latitude region.

The total electron content (TEC) of the ionosphere can be used to study the dynamics of the ionosphere during solar eclipses [7]. By definition, TEC refers to the total number of electrons integrated along the path from the receiver to each GPS, expressed in electrons per square meter, with 1 TEC unit (TECU)= $10^{16} electrons/m^2$. The TEC is one of the most essential ionospheric quantities for many practical applications, and it offers an overall description of ionization in the ionosphere. Since total ionization loss as a result of reduced photoionization during a solar eclipse is an integral measure of ionospheric electron density, reconstructed vertical TEC can offer precise information about total ionization loss [8–10].

Due to the partial or entire blocking of solar radiation, significant depletions in the TEC are expected during solar eclipses compared to a normal day [11]. The ionospheric responses to solar eclipses have been investigated by many researchers using GPS and other measurements, such as rockets, incoherent radar systems, ionosondes, satellite measurements, and theoretical modeling [12]. The continuous operation of a global network of GPS receivers receives signals from a constellation of GPS satellites orbiting the planet in all weather conditions. This provides a chance to study ionospheric activity both regionally and globally in both spatial and temporal domains [2].

According to N. Jakowski et al., [13], GPS TEC measurements in Spain show a significantly reduced ionization during the annular eclipse on 3 October 2005. The ionospheric response during the solar eclipse on March 20, 2015 was investigated using GPS TEC by Hoque et al., [8], and they showed that the percentage TEC depletion depends linearly on solar obscuration. TEC response to the annular solar eclipse of 15 January 2010 was investigated using GPS data by Panda et al., [2], it was shown that there was a sudden collapse of the TEC curve at two stations [Bangalore (IISC) and Hyderabad (HYDE)], which indicates the effect of blocked solar radiation on decayed electron content in the ionosphere over the region.

The objective of this thesis is to study the effect of the partial solar eclipse on the TEC of the ionosphere, and to ensure that the partial eclipse was the cause for the depletion of TEC. In this paper the effects of the partial solar eclipse seen in Addis Ababa and Djibouti on the ionospheric TEC was studied using GPS derived TEC data. The data was taken from the two GPS stations found in Addis Ababa and Djibouti.

This study is organized as follows: The atmosphere and the ionosphere are discussed in chapter two. Chapter three describes the solar eclipse, its types and their effects on the ionospheric TEC. Chapter four is about the data source and methods of analysis. The data availability and the processing method, GPS and GPS related concepts and TEC calculation from GPS data are explained in this chapter. In chapter five the discussion and results are presented. The conclusion and recommendations are briefed in chapter six.

Chapter 2

The Atmosphere and the Ionosphere

2.1 The Atmosphere

The gaseous envelope that surrounds the Earth is known as the atmosphere. It's a relatively steady mixture of numerous different types of gases from various sources. Although molecular Nitrogen and Oxygen account for the majority of the volume, the minor elements carbon dioxide, Water vapor, and ozone play important roles. About 99.96 % of the permanent gases are Nitrogen, Oxygen, and Argon. Carbon dioxide, among the changeable ingredients, can vary in concentration on a localized basis at low levels, water vapor has a wide range of properties. The other primary greenhouse gas, ozone, varies significantly as well [14, 15].

According to the variation in temperature with height, the atmosphere is conventionally divided into layers in the vertical direction. The troposphere, stratosphere, mesosphere, thermosphere, and exosphere are the five layers of the atmosphere. The troposphere is the neutral atmosphere's lowest layer. It is a layer that extends from the ground to roughly 12 km altitude and is bounded above by the tropopause. Temperature in the troposphere falls as height rises, but at some point, the tendency reverses, and temperature begins to rise as height rises. The troposphere is also referred as the lower atmosphere. Most weather phenomena occur here, including cyclones, fronts, hurricanes, rain, snow, thunder, and lightning. The stratosphere is a layer that extends from the tropopause to roughly 50 km altitude and is bounded above by the stratopause. The stratosphere houses the majority of the ozone molecules in the

atmosphere; the ozone layer, which is particularly essential because it absorbs solar ultraviolet (UV) radiation and so protects human and animal life from potentially severe repercussions, is located in the lower stratosphere. The absorption of solar UV photons by molecular oxygen (O_2) in the stratosphere results in the creation of ozone (O_3) molecules, with three O_2 molecules finally becoming two O_3 molecules. The mesosphere, which extends from the stratopause to roughly 85–90 km and is bordered above by the mesopause, is a layer in which temperature decreases with height. The stratosphere and mesosphere make up the middle atmosphere. The thermosphere, which lies above the mesopause, extends from about 90 to 500 kilometers, sees temperature rise with height once more [15,16], is bounded above by the thermopause. The exosphere is found above the thermopause. Where, the pauses are a boundaries that exists between each layer of the atmosphere. The maximum change between the layers occurs at these pauses.

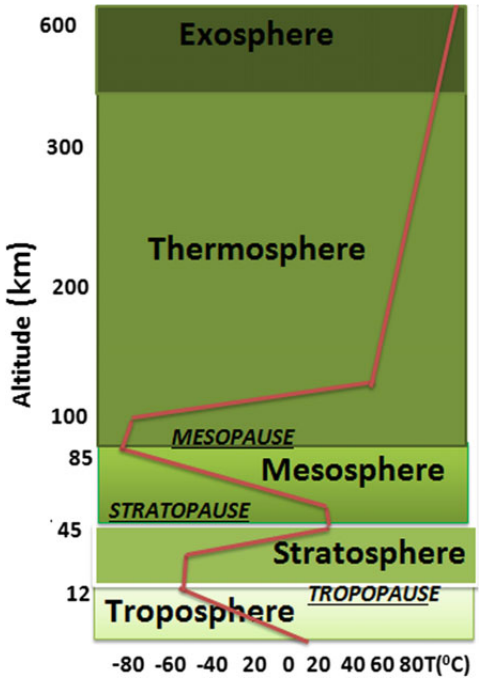

Figure 2.1: Vertical profile of atmospheric temperature indicating the different layers of the Earth's atmosphere [L. R. Cander, 2019]

The upper atmosphere is located above the middle atmosphere, where ionization processes play a larger role in forming atmospheric structure and air becomes so rarefied [15]. Solar rays of infrared, visible, and UV wavelengths are constantly bombarding the environment. Some sun photons are dispersed back to space by atmospheric gases or reflected back to space by clouds or the Earth's surface; others are absorbed

by atmospheric molecules particularly water vapour and ozone or clouds, causing heating of areas of the atmosphere; and still others reach the Earth's surface and heat it. Infrared photons are emitted and absorbed by atmospheric gases (such as carbon dioxide, water vapour and ozone), clouds, and the Earth's surface, resulting in further heat transfer between regions or heat loss to space. As a result, the atmosphere beyond the intermediate atmosphere does not have a consistent composition [14, 15].

2.2 The Ionosphere

Severe UV radiation from the Sun penetrates through the neutral atmosphere. These photons have enough energy to ionize a portion of the neutral atmosphere, resulting in the production of electrons and ions on a continuous basis. The ionosphere is the portion of the atmosphere that is ionized. It is conductive, has a high interaction with radio signals, and can withstand the flow of large electric currents. Therefore, the ionosphere forms as a result of the neutral atmosphere's shielding action against the entrance of particles from the outside. Collisions with the atmosphere absorb the energy of these incoming particles and can cause the ionization of neutral atoms or molecules if their energy is high enough. Photons from the Sun, cosmic rays from the interplanetary medium, or particles from the solar wind or magnetosphere are examples of these particles [16, 17]. The ionosphere is a dynamic environment supporting a large number of plasma instability processes, with substantial implications for global communications and geolocation applications, because it is the region with the highest plasma density in Earth's space environment [18].

2.2.1 Formation of the Ionosphere

The Sun's electromagnetic energy, which extends over the UV and X-ray portions of the spectrum, is the primary cause of ionization in the ionosphere. The intensity of solar radiation as a function of wavelength and the ionization efficiency of neutral atmospheric gases determine the ionization rate at various altitudes. Because the Sun's radiation is gradually absorbed as it passes through the atmosphere, its residual ionizing power is proportional to the length of the atmospheric path, and hence to the solar zenith angle χ. When the Sun is overhead ($\chi = 0$), the ionization rate is highest, but there are geographic, diurnal, and seasonal variations in the ionization density.

Ionization loss processes, primarily collisional recombination of electrons and positive ions, and the attachment of electrons to neutral gas atoms and molecules, balance off the generation of free ionization by solar radiation and charged particles [19].

Photoionization

Free electron–ion pairs are produced by photoionization of neutral gas constituents in planetary atmospheres, and this is the primary source of ionization in most ionospheres. The ionizing photons' energy surpasses the threshold ionization energy in most cases, with the excess going into electron kinetic energy or excitation of the resultant ion. Because the ions are significantly more heavy than the electrons and hence have very little recoil energy during the photoionization process, the electrons pick up the majority of the kinetic energy [20]. The earth's atmosphere is ionized by a broad spectrum of solar X-ray and extreme UV (EUV) radiation [21]. Photoionization, in which a photon imparts enough energy to an atom or molecule to release an electron, is the most common method of ionization in the quiet-time ionosphere. The following is a general description of photoionization processes:

$$X + hv \rightarrow X^{+} + e^{-}$$

where, X is a neutral atom or molecule. This process shows that a high energy photon can ionize a neutral, resulting in an ion and a free electron [16].

Loss Reactions

In low and mid-latitudes, the absorption of solar EUV and X-ray radiation is widely considered as the primary process for the formation of ion-electron pairs. One or more of the major atmospheric elements can be ionized by photons with energy larger than roughly 12 eV. The photon's excess energy is converted into the kinetic energy of the ion-electron pair, and the remaining ionization energy is finally converted to heat during recombination [16, 21]. Recombination is the most common loss mechanism in the ionosphere. The major loss processes are:
The attachment of electrons to neutral molecules;

$$XY + e \rightarrow Y + X^{-}$$

Radiative recombination, when an ion and an electron unite, a neutral and a photon are produced;

$$X^+ + e \rightarrow X + hv$$

Dissociative recombination, when a molecule ion and an electron combine, two potentially excited neutral constituents are formed, such that:

$$XY^+ + e \rightarrow X^* + Y^*$$

Charge Exchange;

$$X^+ + YZ \rightarrow YZ^+ + X$$

After the ion and free electron are produced, a series of chemical reactions occur that ultimately determine which ion species are the most frequent. Charge exchanges are the most essential of these chemical reactions, in which colliding neutral and ionized species exchange charge and possibly dissociate in the process. Non dissociative and dissociative are examples of charge exchange reactions [16, 21].

Non dissociative

$$N_2^+ + O_2 \rightarrow N_2 + O_2^+$$

and

Dissociative

$$O^+ + N_2 \rightarrow NO^+ + N$$

2.2.2 Layers of the Ionosphere

From a chemical standpoint, the atmosphere is tremendously active. The chemical rates in its bottom section, where the neutrals are more dense, can be such that the primary ions are converted into other ionized species almost instantly. These rates may compete with transport processes at higher altitudes [17]. As altitude decreases, EUV light absorption increases, resulting in the establishment of a layer of maximal electron density due to the growing density of neutral molecules. However, due to the different rates of absorption of different molecules and atoms in the atmosphere, a series of distinct regions of electron density occur. Therefore, the upper atmosphere is divided into regions based on the behavior and number of free electrons and other charged particles. These are denoted by the letters D, E, F_1, and F_2. The E layer

being the first to be detected [20, 22].

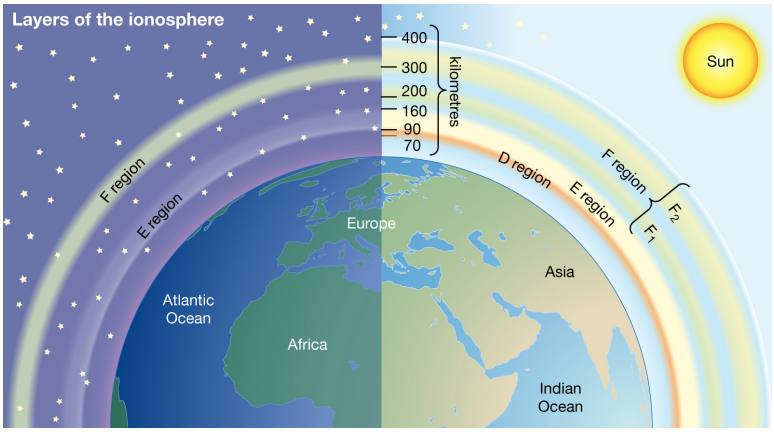

Figure 2.2: Layers of the ionosphere [https://www.britannica.com/science/F-region]

The D Layer

The D layer is the lowest part of the ionosphere, located at a height from around 70 to 90 kilometers. It has a low electron density, which appears immediately after sunrise and disappears shortly after nightfall. Solar X-rays, which cause ionization of the major neutral gases N_2 and O_2, and intense solar Lyman-radiation (wavelength = 121.5nm), which causes ionization of the nitric oxide NO, are the primary sources of photoionization in this region. The D layer is controlled by chemical processes and the dominant species are molecular ions and neutrals. It contains both positive and negative ions, as well as water cluster ions. At altitudes below 85 km, cluster ions dominate the D region, and they are generated by hydration of the main ions NO^+ and O_2^+ [20, 23].

The chemistry of the D region is caused by two pathways. First, the Lyman emission line is insufficiently energetic to ionize the thermosphere's primary neutral, therefore it is not halted above 90 km and reaches the region below. The Nitric oxide NO is present below 90 km and has a 9.6 eV ionization potential, allowing Lyman to ionize the molecule. Although NO is a very minor constituent of the atmosphere, the intensity of this line is such that a significant amount of NO^+ ion is created. Besides this, O_2^+ ion is still created at a comparable level. The electron affinity of molecular oxygen O_2 is high, which could lead to an electron attachment via the ternary reaction [17].

$$O_2 + e^- + M \rightarrow {O_2}^- + M$$

where, M denotes a molecule N_2 or O_2. This method likewise works in the case of atomic oxygen O. These processes lead to the creation of negative ions ${O_2}^-$ and O^-. The electron detachment reaction is the most basic method for removing ${O_2}^-$ ions.

$$ {O_2}^- + O \rightarrow O_3 + e^- $$

Positive ions, negative ions, and electrons coexist at concentration levels that ensure quasi-neutrality in the D region. The electrons may vanish under certain conditions, primarily at night, and the charge balance between positive and negative ions results in quasi-neutrality. During the day, chemistry removes all negative ions, and electrons maintain quasi-neutrality.

The E Layer

The E layer stretches from 90 to 140 kilometers, with a high near 110 kilometers. The ionosphere is dominated by molecular ions ${O_2}^+$ and NO^+ below 200 km. Photoionization of neutral diatomic oxygen produces ${O_2}^+$, while a rapid charge exchange mechanism between primary ions O^+, ${N_2}^+$, and ${O_2}^+$ produces NO^+. In the E region NO^+ and ${O_2}^+$ disappear mostly through dissociative recombination, which generates unstable intermediate molecules before separating into the individual neutral atomic species [17, 23]. The production of ${O_2}^+$ results mainly from the ionization of its neutral parent O_2 and the charge exchange reaction with ${N_2}^+$ and NO^+ is a chemical byproduct formed mostly by an ion charge exchange reaction with ${N_2}^+$ and O^+.

$$ {N_2}^+ + O \rightarrow NO^+ + N $$

$$ O^+ + N_2 \rightarrow NO^+ + N $$

The reactions that involve ${N_2}^+$ have a significant impact on its concentration, and despite the fact that its neutral parent N_2 is the most abundant neutral, ${N_2}^+$ is a minor ionosphere species. Dissociative electron recombination almost completely balances the creation of molecular ions.

$$ {O_2}^+ + e^- \rightarrow O + O $$

and

$$ NO^+ + e^- \rightarrow N + O $$

The recombination rates of these processes are determined by the electron thermal energy. The electron concentration is likely to rise if electrons are heated by plasma instability or strong currents [17].

The F_1 Layer

The generation of ${N_2}^+$ and O^+ ions, which are sources for the NO^+ ion, is prominent around 150 km. This corresponds to the F_1 region, which stretches from roughly 140 kilometers up to 200 kilometers. Above 180 km, electron recombination no longer dominates the chemistry, which corresponds to a change from molecular to atomic ions [17]. The atomic oxygen ion, O^+ becomes the dominating ion over 180–200 km. Since atomic oxygen ions rarely lose their charge through radiative recombination, they must first be transformed to molecular ions, which then lose their charge through the dissociative recombination process. The EUV light is the primary source of ionization in the F_1 layer. Because electron densities are primarily controlled by the sun's zenith angle, the F_1 layer is only visible during the day [22, 23].

The F_2 Layer

The F_2 layer extends from 200 up to 400 kilometers. Diffusion is the only process capable of balancing ion generation above 300 kilometers. The conflict between the creation of O^+ and the diffusion of this ion through the neutral atmosphere defines the F_2 ionospheric layer, which is thus defined by these processes. This layer reaches its maximum between 250 and 400 kilometers [22]. The diurnal and latitudinal changes in electron density are not affected by the solar zenith angle. The rate of electron loss in the F_2 layer is determined by the concentration of molecular ions, mainly O_2 and N_2, whereas the rate of production is determined by the concentration of atomic oxygen O^+ [24], which is the dominant ion in this region. From the perspective of navigation and space communication, the F_2 region is the most essential. It's also the region with the most variability and irregularity in terms of forecasting. The electron concentration peaks in these region and remains constant throughout the day and night [23].

2.3 Geographic Regions of the Ionosphere

The location of the Sun, the Earth's magnetic field, and atmospheric winds that can transfer ionization and charged particles between hemispheres are all factors that influence ionospheric features. The impacts of these inter-dependencies give rise to different geographic regions [19]. Therefore, ionospheric behavior can be divided into three geographic regions: (1) high latitudes with geomagnetic latitudes between 90 and 60 degrees; (2) mid latitudes with geomagnetic latitudes between 60 and 20 degrees; and (3) low latitudes with geomagnetic latitudes between 0 and 20 degrees. The auroral and polar cap regions at high latitudes, as well as the equatorial and equatorial anomaly regions in low latitudes, are sub-regions of these main regions [24].

Equatorial and Low Latitude

The Earth's magnetic field is horizontal at the geomagnetic equator. Near the equator, electric fields become more important, creating vertical ionization drifts [19]. The largest values of the peak-electron density, as well as the most pronounced amplitude and phase scintillation effects, can be found in the equatorial region. The combined action of the sun's high radiation output and the earth's electric and magnetic fields causes electrons to rise and move along the magnetic field's horizontal lines [22].

Mid Latitude

The mid-latitude region has the least extreme behavior of all the geographic regions. Because the magnetic field at mid latitudes is neither vertical nor horizontal. It is usually free of the impact imposed by the equatorial region's horizontal magnetic field geometry [19, 22].

High Latitude

Collisional ionization, in addition to photonionization, is a source of ionization in the high-latitude region. The fundamental reason for this is that the geomagnetic field lines in this region are nearly vertical, allowing charged particles to sink to E layer altitudes about 100 km, resulting in an ionosphere that is significantly more complicated than that found at mid and low latitudes [22, 23].

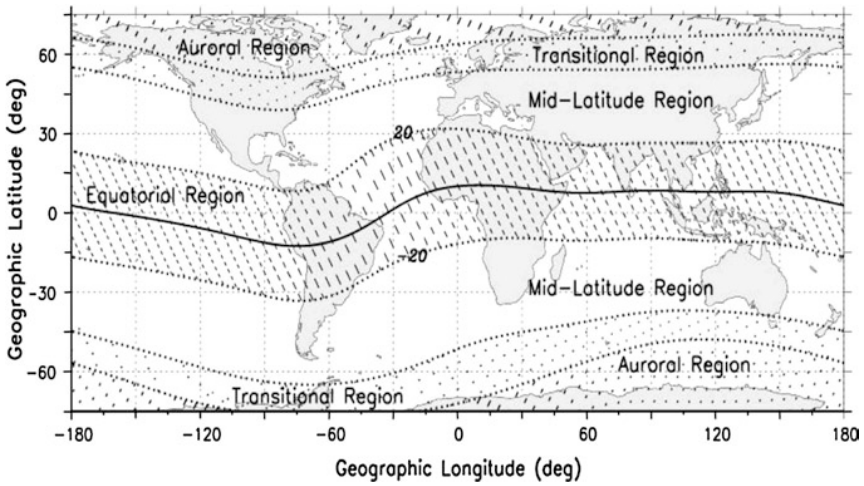

Figure 2.3: The major geographic regions of the ionosphere [B. Zolesi and L. R. Cander, 2014]

2.4 Geomagnetic Indices

Current systems, which are generated by regular solar radiation fluctuations, produce daily regular magnetic field variations. Magnetic fields are also created by other irregular current systems. The interaction of the solar wind with the magnetosphere, the magnetosphere itself, the interactions between the magnetosphere and the ionosphere, and the ionosphere itself all produce changes. Magnetic activity indices were developed as a result to explain changes in the geomagnetic field caused by irregular current systems. The planetary index (Kp), disturbance storm time (Dst), and Ap indices are all indicators of geomagnetic activity [25].

The Dst is a magnetic activity indicator that measures the intensity of the globally symmetrical equatorial electrojet, also known as the ring current, and is generated by a network of geomagnetic observatories around the equator. Kp Index is a measure of geomagnetic activity in the Earth's atmosphere. 13 observatories between 46 and 63 degrees north and south geomagnetic latitude determine their own integer K ranging from 0 to 9 for each 3 hour period of the day based on measured ranges in the geomagnetic field components. Kp values from 0 to 3 indicates lower magnetic activity, and values above 5, indicates storm. The Kp index is used to calculate the 3-hourly Ap index. The range of the most disturbed of the three field components is called Ap. The Ap index measures geomagnetic activity on a daily basis [22, 25].

Chapter 3

The Solar Eclipse

The eclipse is a beautiful occurrence caused by the Earth's, Sun's, and Moon's orbital interactions. There are two types, lunar and solar. Lunar eclipses occur when the Earth's shadow falls on the Moon, darkening it when viewed from Earth [26]. A solar eclipse occurs when the Moon passes in a direct line between the Earth and the Sun. The Moon's shadow travels over the Earth's surface and blocks out the Sun's light as seen from the Earth. Every month, a new Moon occurs when the Moon passes between the Earth and the Sun, casting a shadow on the near side of the Moon. Normally, the Earth and Moon aren't aligned enough to generate an eclipse; but, about once every 6 months, the Sun, Moon, and Earth are aligned well enough for the Moon's shadow to fall on the Earth [27].

There are mainly three types of solar eclipses; total solar eclipse, annular solar eclipse and partial solar eclipse. The Moon may or may not be large enough to block out the entire solar disk as it passes between the Earth and the Sun. Because its orbit is not round, it passes closer to the Earth at perigee and farther away at apogee. When it is close to perigee, its disk appears to be relatively huge, allowing it to totally cover the Sun in a total eclipse. Because its disk seems smaller at apogee, it is unable to completely obscure the Sun, an annular eclipse occurs and a bright annulus appears around the circumference of the Moon [28].

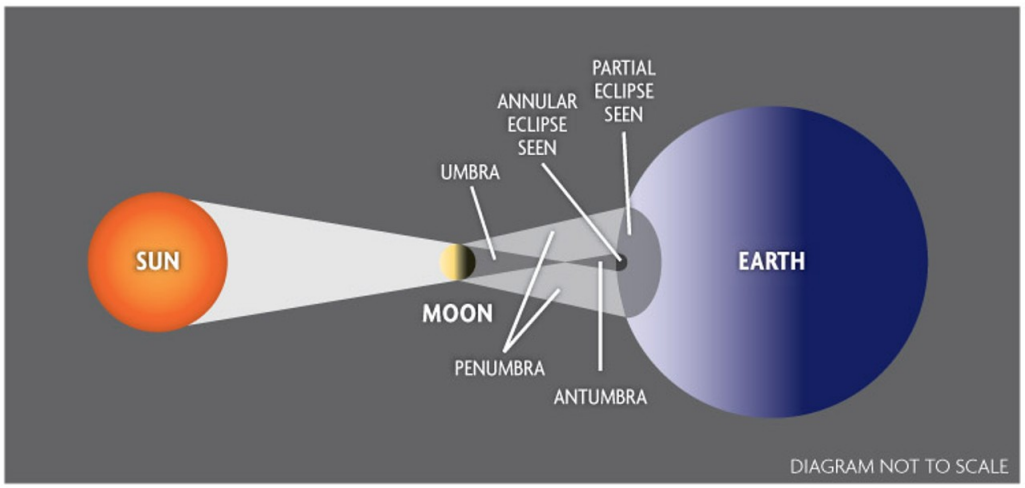

Figure 3.1: Geometry of a solar eclipse [https://www.northcoastjournal.com/ring-of-fire]

The type of eclipse we see is determined by the type of shadow as shown in the above figure. The umbra is the dark center of the shadow, whereas the penumbra and antumbra are two forms of half shadows. The umbra is the first shadow cast and the Moon's shadow's dark center. As it approaches the Earth, it becomes smaller. The umbra is a completely shaded zone where the Moon entirely covers the solar disk as observed from anywhere within that narrow region. The umbral spot has a radius of tens of miles. The Moon only partially obscures the Sun all around the zone of totality, which is referred to as the penumbra. The penumbra is the second shadow, it is significantly larger than the umbra and it grows greater as it approaches the Earth. The penumbral spot has a radius of 2,000–2,200 miles. Anywhere throughout that broad area, a partial eclipse will be seen, with a grazing contact between the lunar and solar disks occurring at the very edge. The third shadow is an antumbra, an annular eclipse occurs when the antumbra strikes the Earth's surface [28, 29].

3.1 Annular Solar Eclipse

Because the Moon is at its farthest distance from the Earth, an annular solar eclipse occurs when the Sun and Moon are perfectly aligned, but the Moon seems to be smaller than the Sun. During an annular eclipse, the Sun appears as a bright ring surrounding the Moon's dark disk. This means that the Moon is too small to entirely obscure the Sun, thus even though it is directly in front of it, a ring of visible Sun can be seen

around the Moon's edge. The tip of the umbral shadow does not reach the Earth's surface during an annular eclipse. Before they hit the Earth's surface, the lines diverge out again beyond the sharp edge of the umbra, when the shadow track becomes infinitesimally thin. This third shadow is called an antumbra. The silhouette of the lunar disc appears in front of the brilliant solar disc when the antumbra strikes the Earth's surface, forming an annular eclipse [29].

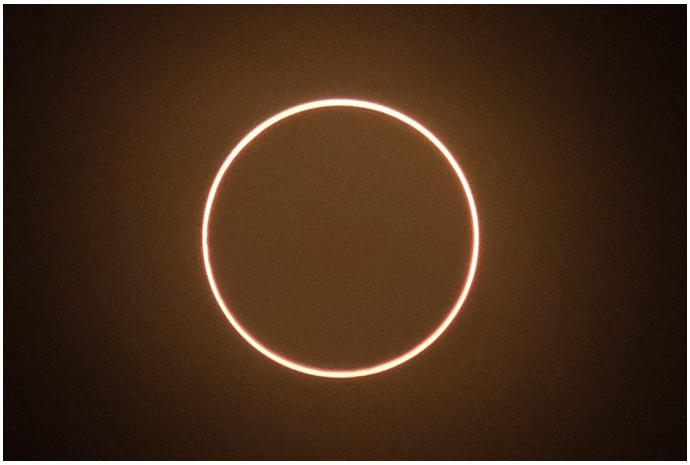

Figure 3.2: Annular solar eclipse [https://www.wikiwand.com]

3.2 Total Solar Eclipse

When the angular diameters of the Sun and the Moon as seen from Earth are almost equal, a total solar eclipse occurs. The apparent sizes vary, however, because the distance between the Earth and the Sun varies over the year, and the distance between the Moon and the Earth varies month to month. To attain totality, the Moon must be close enough to the Earth and the Sun must be far enough away from the Earth for the lunar disk to fully block the Sun. Every 18 months or so, a total solar eclipse happens somewhere on the earth [28]. When the total eclipse hits Earth, the individuals who view it are in the heart of the moon's shadow. As if it were night, the sky darkens dramatically.

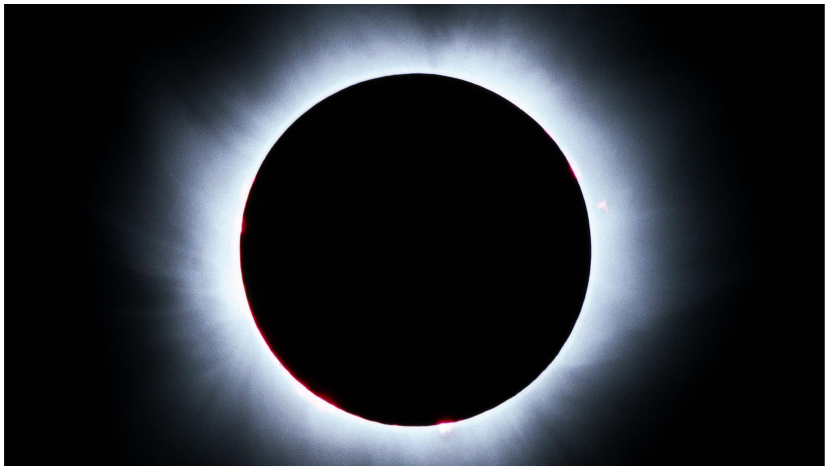

Figure 3.3: Total solar eclipse [https://www.dlr.de/content/en/images/2017/3/the-magical-moment-of-totality-the-solar-corona-becomes-visible-27930.html]

When the Moon's black shadow completely obscures the Sun's intensely bright light, the solar corona, which is considerably fainter, is revealed. The umbra is the smaller inner section of the Moon's shadow; observers in this area will see the Sun fully obscured by the Moon, resulting in a total eclipse of the Sun. The corona, which is derived from the Latin word for "crown," surrounds the Moon's circumference. This is a solar structure visible only during an eclipse, far beyond the Moon.

3.3 Partial Solar Eclipse

Apart from the totality stage, there is a long period of partial eclipse that precedes and follows the main event, lasting some hours. This is the amount of time it takes for the Moon to gradually cover the Sun before uncovering it later [28]. The umbra sometimes misses the Earth entirely, while the penumbra, which is wider, does not. In this instance, a partial eclipse may be visible in a few regions. When the Sun, Moon, and Earth are not perfectly aligned, a partial solar eclipse occurs and the Moon only partially obscures the Sun. Only a small portion of the Sun's surface appears to have a black shadow.

Figure 3.4: Partial solar eclipse [https://www.bostonglobe.com/2021/06/08/metro/how-see-june-10-annular-solar-eclipse-rhode-island/]

The penumbra is the outermost and greatest component of the Moon's shadow. Any observers in this area will notice that only a portion of the Sun is obscured by the Moon, resulting in a partial eclipse of the Sun. As it travels over the Earth, the penumbra is quite large, usually a few of thousand miles across.

3.4 The June 21, 2020 Annular Solar Eclipse

An annular solar eclipse occurred on June 21, 2020. The annular eclipse began in Africa for the Congolese people and continued over South Sudan, Ethiopia, Djibouti, Yemen, Oman, Saudi Arabia, the Indian Ocean, and Pakistan before entering India over Rajasthan. It then travels to Tibet, China, and Taiwan before arriving at the Pacific Ocean's midsection. The annular eclipse first appeared in the Republic of Congo a few minutes after sunrise, at 5:56 local time, resulting in an almost-complete blackout that lasted a minute and 22 seconds. The astronomical phenomena then traveled eastwards over Africa and Asia until peaking in the southern and northern parts of Asia as a maximum eclipse. At 12:10 AM, local time, it was seen in Uttarakhand, India, close the Chinese border. In this section of the world, the precise alignment of the Earth, Moon, and Sun was also visible for 38 seconds. Ethiopians, Indians, and Pakistanis were all able to see the annular eclipse. Around 8:32 a.m., the scenery was last seen in regions of China. Just before sunset, a partial eclipse was seen across much of the rest of Africa, southeastern Europe, much of Asia, New Guinea, and northern Australia.

The following figure depicts regions where the annular solar eclipse of 2020 June

21 was visible. Partial eclipse occurred over Africa, southeast Europe and Asia and annular eclipse occurred over central Africa, south Asia, China and Pacific.

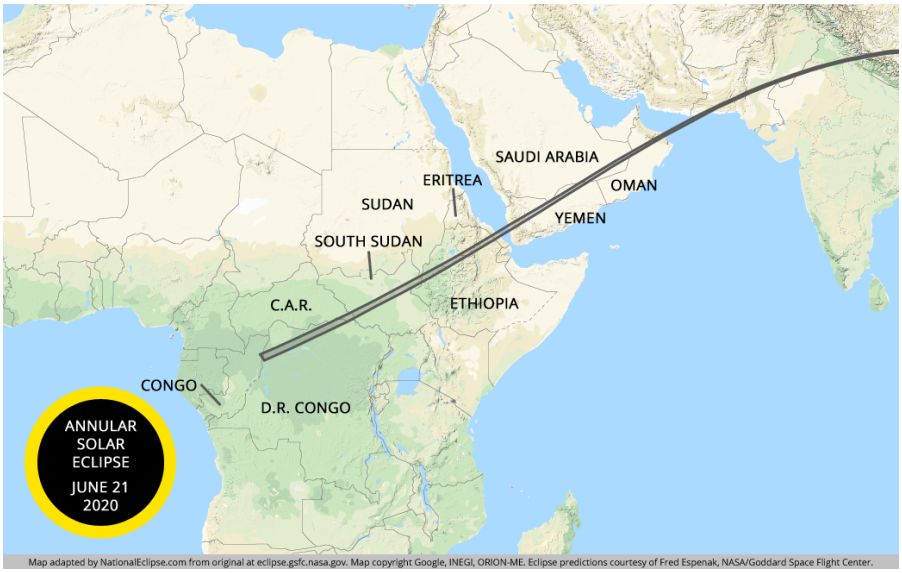

Figure 3.5: Annular solar eclipse 2020, June 21 [https://nationaleclipse.com]

The Eclipse was partial over the regions Addis Ababa and Djibouti. The coverage of the sun was 89.13% over Addis Ababa and 89.47% over Djibouti. The partial eclipse over Addis Ababa begins at 06:49:46 AM, its maximum was at 07:56:51 AM and it ends at 09:15:37 AM local times. The eclipse duration was 2 hours 25 minutes and 51 seconds. The partial eclipse over Djibouti begins at 06:52:14 AM, its maximum was at 08:02:30 AM and it ends at 09:25:51 AM local times. The eclipse duration was 2 hours 33 minutes and 37 seconds. The local times are the East African Time (EAT) for Addis Ababa and Djibouti, given by UT+3.

3.5 Effects of the Solar Eclipse on TEC

Solar eclipses are natural occurrences in which the Moon blocks the Sun entirely or partially, casting a shadow across the Earth. They offer a once in a lifetime opportunity to investigate a variety of phenomena in the Earth's upper and lower atmosphere caused by a temporary decrease in the flux of heating and ionizing radiation [30]. Ionization of the ionospheric layer is thought to be mostly induced by solar radiation. The Moon blocks a portion of the solar radiation from reaching the Earth during the eclipse. There will be a decrease in ionospheric ionization as a result of this action. This results in

a decrease in the amount of electrons in the ionosphere, and thus a decrease in the amount of TEC [9].

An eclipse affects all ionospheric levels, though the effects vary in strength and appearance. The amount of ionization is governed by ion production and loss processes in the D, E, and F_1 regions. Thus, during the eclipse time, the optical rays are hidden, resulting in a direct reduction in photoionization, the destruction of the photochemical equilibrium, and the depletion of the electron density, showing that over short time scales, variations in solar radiation affects the TEC. The topside regions are more influenced by plasma redistribution processes, because the F_2 layer is driven by photochemical processes as well as electrodynamical and neutral forces, its behavior may be quite different. Transport processes are extremely significant in this region [12, 30–32].

Maximum TEC reduction occurred several minutes after the maximum obscuration, showing that the recombination process was still in progress, the transport time scales and the delayed response of the upper ionosphere. The magnitude of the eclipse, which is directly related to the photoionization process, is proportional to the amount of TEC reduction [7].

Chapter 4

Data Source and Methods of Analysis

4.1 Data Source

4.1.1 Global Positioning System (GPS)

The Global Positioning System (GPS) is a United States owned service that delivers positioning, navigation, and timing services to users [33]. The space segment, the control segment, and the user segment are the three components of the GPS system. The space and control segments are developed, maintained, and operated by the United States space force.

A constellation of satellites transmits radio signals to users, making up the GPS space segment. The United States has committed to having at least 24 operable GPS satellites available 95% of the time. GPS satellites orbit the Earth at a height of around 20,200 kilometers in medium Earth orbit (MEO), each satellite circles the Earth twice a day. The GPS constellation's satellites are grouped in six evenly spaced orbital planes around the Earth. The baseline satellites occupy four slots on each plane. This 24-slot configuration assures that users can see at least four satellites from almost anywhere on the earth [34].

The control segment consists of a global network of master control, data uploading, and monitoring stations. These stations receive a satellite's signal and compare it to orbit models that show where the spacecraft should be. Operators at these stations can change the location of satellites to correct or vary their orbital paths, such as if

a satellite has drifted or needs to be repositioned to avoid colliding with debris. The GPS control segment is made up of a worldwide network of ground stations that track GPS satellites, monitor their broadcasts, conduct analysis, and relay commands and data to the constellation. A master control station, an alternate master control station, 11 command and control antennas, and 16 monitoring locations make up the current operational control segment.

The user segment is the equipment that receives satellite signals and outputs a position based on the time and orbital location of at least four satellites. This portion includes the user's antennas, which are used to locate and receive high quality signals, as well as high precision receivers and positioning engines, which process the signals and correct any potential timing problems.

GPS Signals

The GPS signal is an electromagnetic wave delivered by GPS satellites that is generated by an oscillating electric force. GPS satellites currently broadcast range codes and navigation data on two frequencies, L_1 and L_2 [35]. The C/A (course acquisition) code, the P (precise) code, and the navigation message are the three types of coding present on carrier signals. The C/A code can be found on the L_1 channel and the P code is identical on both the L_1 and L_2 channels. Whereas, the C/A code is good for early signal locking, but the P code is preferable for more precise positioning. The navigation message can also be found on the L_1 channel. The broadcast ephemeris, satellite clock corrections, almanac data, ionosphere information, and satellite health status are all included in the navigation message. A GPS satellite's signals are fundamentally driven by atomic clocks, $10.23Mhz$ is the fundamental frequency. By multiplying the frequency by 154 for the L_1 channel ($frequency = 1575.42Mhz$) and 120 for the L_2 channel ($frequency = 1227.60Mhz$), two carrier signals, which can be thought of as sine waves, are formed from this signal [36].

GPS Observables

The three fundamental GPS observables are the pseudo-range, carrier phase and Doppler measurement. The pseudo-range observable is the geometric range between the GPS satellite and the GPS receiver based on time measurements scaled by the speed of light, which is disrupted by the lack of synchronization between the satellite and receiver

clocks, as well as the propagation media. The GPS receiver calculates the distance between the satellite and the receiver by measuring the time it takes for the signal to travel from the satellite to the receiver. This temporal offset multiplied by the speed of light gives the pseudo-range. The carrier phase is the difference between the phases of received carrier signal and a reference signal generated by the receiver's internal oscillator. The fractional phase is measured by the receiver, which maintains track of changes in the phase. The carrier phase rate is measured by the Doppler measurement [37, 38].

GPS Error Sources

Orbital errors, satellite and receiver clock errors, tropospheric and ionospheric delays, receiver noise, and multipath are all examples of GPS errors. The uncertainty of the predicted ephemerides and Selective Availability (SA) cause orbital inaccuracy. The GPS satellites employ atomic clocks to keep a very accurate GPS time. The difference between satellite clock time and true GPS time is known as the satellite clock error and the offset of the receiver clock time with respect to GPS time is known as receiver clock error. The receiver clock error is determined by receiver hardware and can be calculated as an unknown parameter or reduced by comparing two receivers. The refractions of a GPS signal in the lower atmosphere generate the tropospheric delay. A variety of factors influence the degree of this inaccuracy, including temperature, humidity, pressure, and the type of terrain beneath the signal path. Multipath refers to a GPS signal that bounces off a reflecting surface before reaching the GPS receiver antenna [38]. There is a delay in the GPS code pseudo-range and an advance in the carrier phase pseudo-range due to the existence of free electrons in the ionosphere. Both refraction and dispersion influence GPS signals as they pass through this layer. The effect of the ionosphere is determined by the TEC along the GPS signal path. The ionosphere's effect can be measured using dual frequency measurements and the ionosphere's dispersive nature. Therefore, dual frequency correction techniques can eliminate the majority of ionospheric error [37, 39].

4.1.2 Total Electron Content (TEC) From GPS Data

Ground based or space based devices have been used to learn more about the ionosphere. The GPS is one of the tools that has been widely employed for this pur-

pose. GPS data enable the investigation of dispersive propagation properties of the ionosphere for trans-ionospheric radio wave propagation for ionospheric characterization [40]. The atmosphere delays signals from satellites orbiting the earth as they travel to earth-bound receivers. The ionosphere, a layer of the atmosphere characterized by an excess of free electrons, is responsible for a significant portion of this delay. TEC is a measure of ionospheric density that can be used to remove ionospheric delay from satellite signals and to drive models that attempt to anticipate or research this region. The GPS constellation has been used to calculate TEC since the 1990s, despite its primary use as a location tool [41].

The accumulated effect by the time the signal arrives at the reception determines the integrated TEC from the receiver to the satellite. The ionospheric delay must be taken into account when using GPS to obtain extremely precise positions. The GPS uses two frequencies as explained.

$$f_1 = 1575.42MHz$$

and

$$f_2 = 1227.60MHz$$

The difference in ionospheric delays between the L_1 and L_2 GPS frequencies, which are commonly considered to travel along the same path through the ionosphere, can be measured using a dual frequency GPS receiver [10]. The dispersive behavior of the ionosphere affects both the code and phase measurements by a similar factor, but with opposite signs [22].

The absolute value of the group delay is given by:

$$I = \int \frac{X}{2} ds = \frac{40.3}{f^2} \int N_e ds$$

The TEC is:

$$TEC = \int N_e ds$$

Where, the TEC characterizes the delay. Which gives:

$$I = \frac{40.3}{f^2} TEC$$

The group delay for the dual frequency (L_1, L_2) observation can be calculated as follows using the above equation.

$$P_1 - P_2 = 40.3.TEC \left(\frac{1}{f_2^2} - \frac{1}{f_1^2} \right)$$

Where $P1$ and $P2$ are the group path lengths for the high ($f1$ =1575.42 MHz) and low ($f2$ =1227.6 MHz) GPS frequencies, respectively. As a result, the following is the group TEC for dual frequency GPS measurement:

$$TEC = \frac{1}{40.3}\left(\frac{f_1^2 f_2^2}{f_1^2 - f_2^2}\right)(P_2 - P_1)$$

Similarly, the relative phase TEC can be calculated using the equation:

$$TEC = \frac{1}{40.3}\left(\frac{f_1^2 f_2^2}{f_1^2 - f_2^2}\right)(\phi_1 - \phi_2)$$

where ϕ_1 and ϕ_2 are phases of carriers $L1$ and $L2$, respectively.

The above calculated TEC is known as slant TEC (STEC). STEC is a measure of the TEC of the ionosphere along the ray path from the satellite to the receiver [10]. It is desirable to compute an equivalent vertical value of TEC (VTEC) that is independent of the ray path's height because it is a quantity that is dependent on the geometry of the ray path [42]. The STEC values are then converted to absolute VTEC values using a simple mapping function and allocated to an ionospheric pierce point (IPP) latitude and longitude, assuming the ionosphere is compressed into a thin shell (SLIM or thin layer model), as illustrated in the following figure [2].

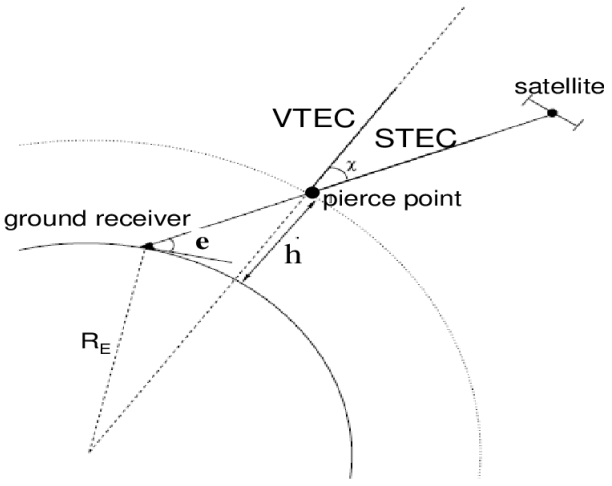

Figure 4.1: Geometry for the conversion of STEC to VTEC [J. Shim, 2009]

The ionospheric pierce point, which is the intersection of the line of sight ray and the thin shell at altitude h, is attributed to the VTEC values. Where, VTEC refers to TEC calculated on a vertical path in the local zenith direction [43]. Using the explained mapping function, VTEC is derived from STEC as follows [44]:

$$VTEC = M(e) \times STEC$$

Where,

$$M(e) = \left[1 - \left(\frac{cos(e)}{1 + (\frac{h}{R_E})}\right)^2\right]^{\frac{1}{2}}$$

Where, e is an elevation angle of a satellite, h is ionospheric shell height, and R_E is the Earth's mean radius. The curvature of the Earth is taken into account in this mapping function [45].

4.2 Data and Methods of Analysis

Dual frequency GPS observations were used to derive TEC in this paper. TEC data was collected from two GPS stations found in Addis Ababa and Djibouti, to show the effect of the partial solar eclipse on the ionospheric TEC. Two days before, two days after and the day during the eclipse and three years of June 21, TEC data were used for each station. The following table shows the geographic and geomagnetic latitude and longitude of ADIS and DJIG stations. ADIS is a station found in Addis Ababa and DJIG is a station found in Djibouti.

Table 4.1: Geographic and geomagnetic regions of the two stations

Staions	Geog. Lat	Geog. Long	Geomag. Lat	Geomag. Long
ADIS	9.03°N	38.76°E	5.44°N	112.55°E
DJIG	11.52°N	42.84°E	7.28°N	116.91°E

To study the relationship between the decrease in TEC and the partial solar eclipse, data was taken from two GPS stations (ADIS and DJIG) from the University NAVSTAR Consortium (UNAVCO) database (https://www.unavco.org) and the crustal dynamics data information system (CDDIS) database (https://cddis.nasa.gov/). The data from each receiver was in Receiver Independent Exchange Format (RINEX) and needed to be converted to TEC. To get the proper TEC parameters, the format conversion was processed using GPS-TEC software developed by Gopi Seemala [46]. Only signals from satellites with an elevation angle greater than 20 degrees were included in the analysis. Filtering was done by the software to eliminate disturbances like multipath, noises from high-rise buildings or tall trees, and other sources that aren't related to ionosphere effects. After processing with the GPS-TEC Software, the VTEC data was plotted using MATLAB software.

The Dst index data was obtained from the geomagnetic equatorial Dst index home page (http://wdc.kugi.kyoto-u.ac.jp/dstdir/) and the Kp index data was taken from the International Service Of Geomagnetic Indices(ISGI) website (http://isgi.unistra.fr/). The data for the magnitude and obscuration of solar eclipses were taken from NASA's Eclipse Map website (https://eclipse.gsfc.nasa.gov).

Chapter 5

Results and Discussion

The ionospheric TEC response for the partial solar eclipse was investigated using two GPS stations found in Addis Ababa and Djibouti, which are located in the low latitude East African region. Data taken from the two stations were used to analyze the effects of the partial solar eclipse in the variation of the TEC. The GPS TEC measurements taken at each station during the solar eclipse were compared to the TEC measurements taken at the same time the days before and after the eclipse, because the influence of the solar eclipse on TEC fluctuations can be studied using a time series of TEC values from the day before, during, and after the solar eclipse [1]. Three years of June 21 data were taken to make sure that the observed depletion were not due to a daily variation.

All the selected days were a quite days in which the geomagnetic and solar activities were low, but June 2020 was the quietest of all. TEC values of the selected years are different than the June 2020, but the eclipse being in the morning time helped to compare the depletion properly. The Dst and Kp indices were studied during the selected days. The Dst were more than -20 nano Tesla (nT), while the Kp values were 3 and below 3 as shown in the figures (5.1-5.12), indicating no magnetic storm was observed. The Dst and the Kp values demonstrated that geomagnetic activities had no impact on ionospheric conditions during the eclipse. The eclipse occurred at the start of the 25th solar cycle, during the solar minimum. It's advantageous because the ionosphere's impact from space weather was minimum [11].

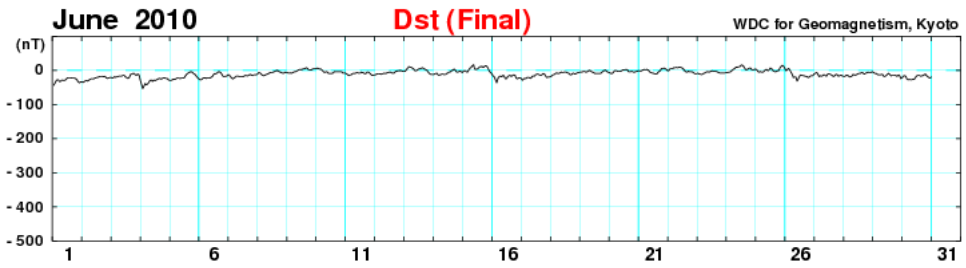

Figure 5.1: Dst index June 21,2010

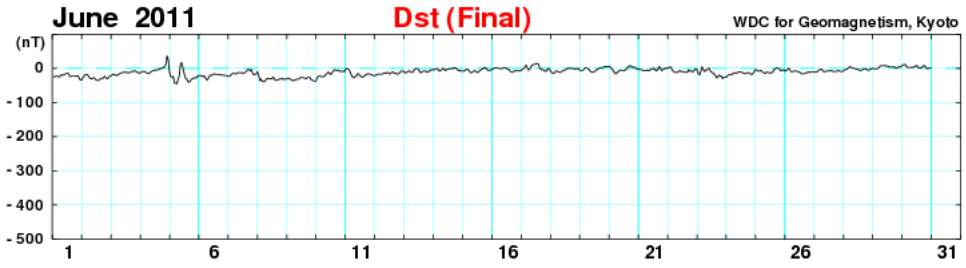

Figure 5.2: Dst index June 21,2011

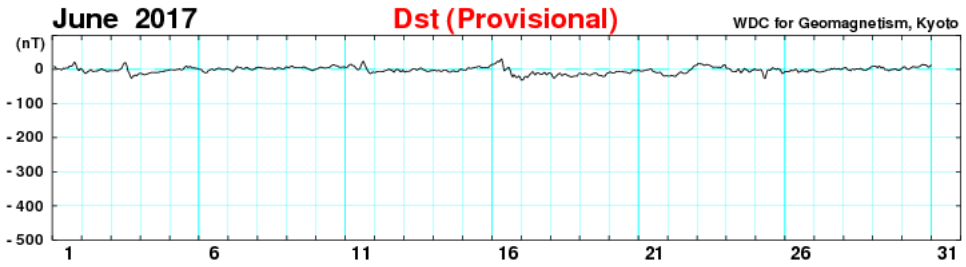

Figure 5.3: Dst index June 21,2017

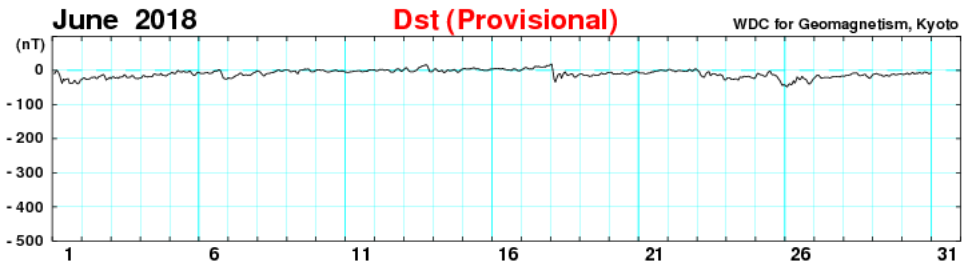

Figure 5.4: Dst index June 21,2018

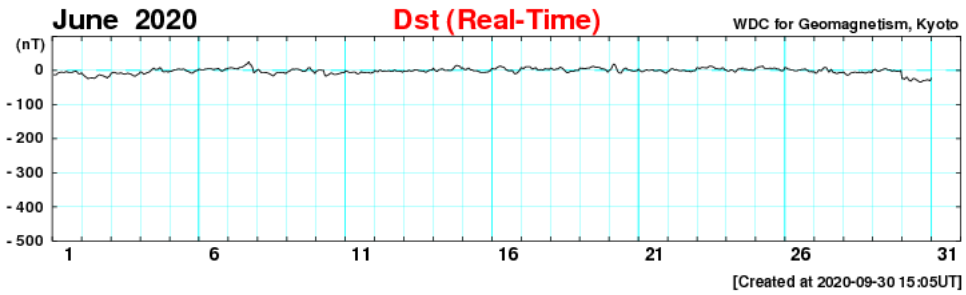

Figure 5.5: Dst index June 21,2020

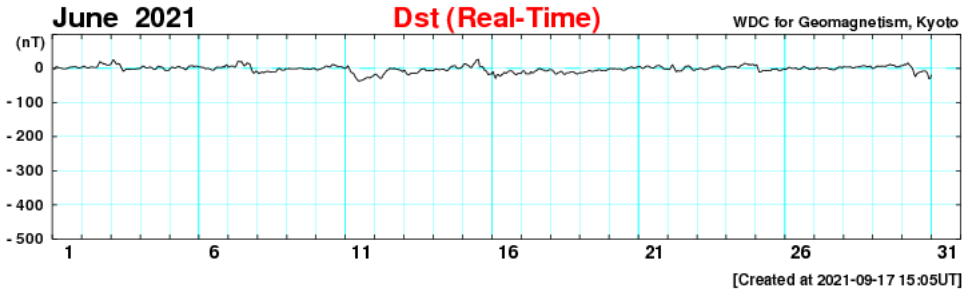

Figure 5.6: Dst index June 21,2021

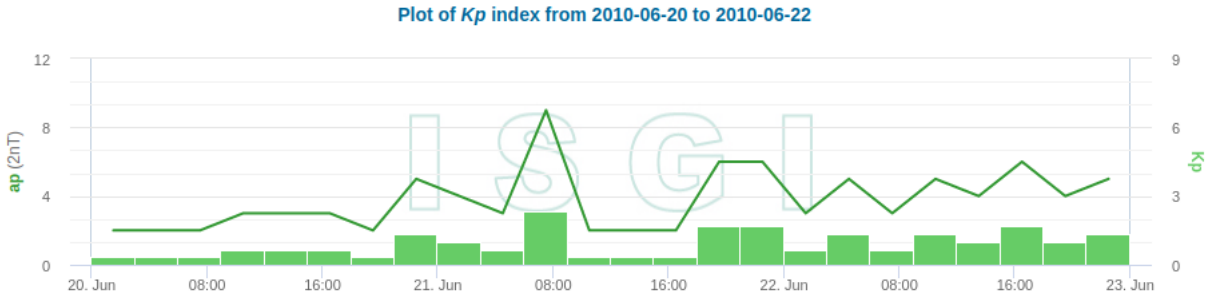

Figure 5.7: Kp index June (20-22), 2010

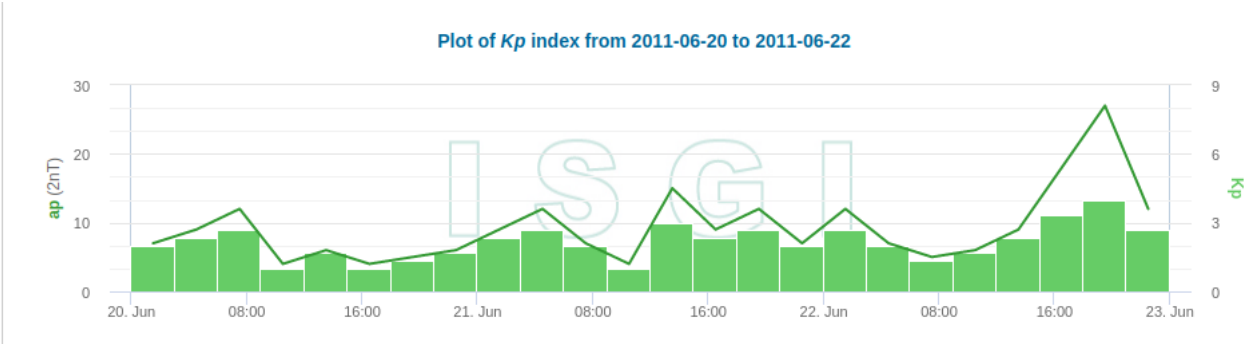

Figure 5.8: Kp index June (20-22), 2011

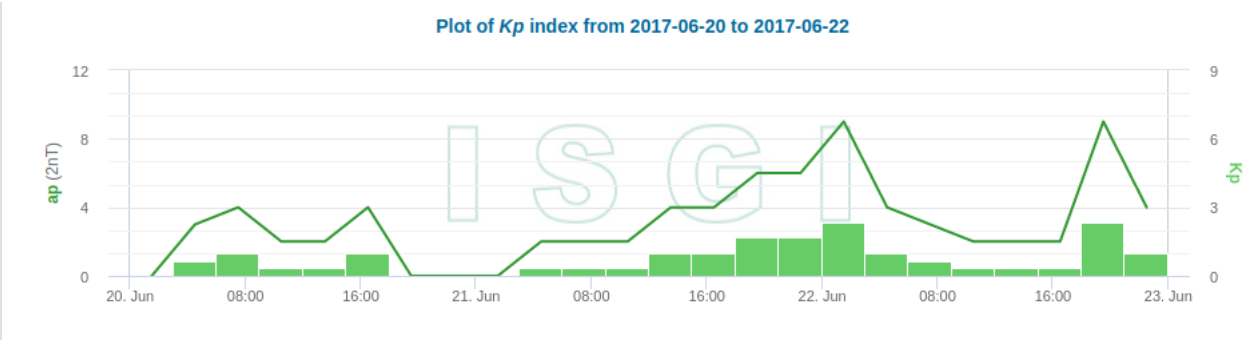

Figure 5.9: Kp index June (20-22), 2017

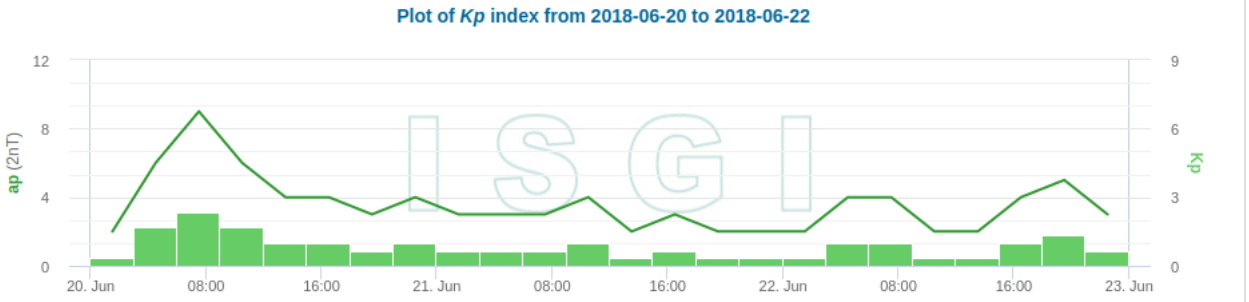

Figure 5.10: Kp index June (20-22), 2018

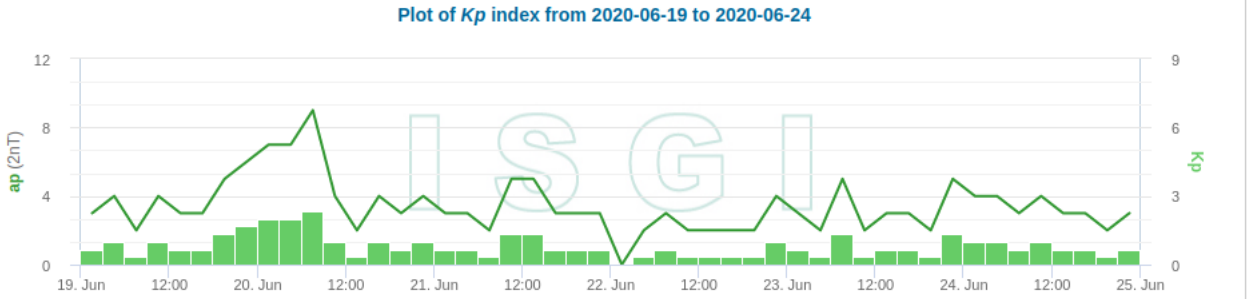

Figure 5.11: Kp index June (19-24), 2020

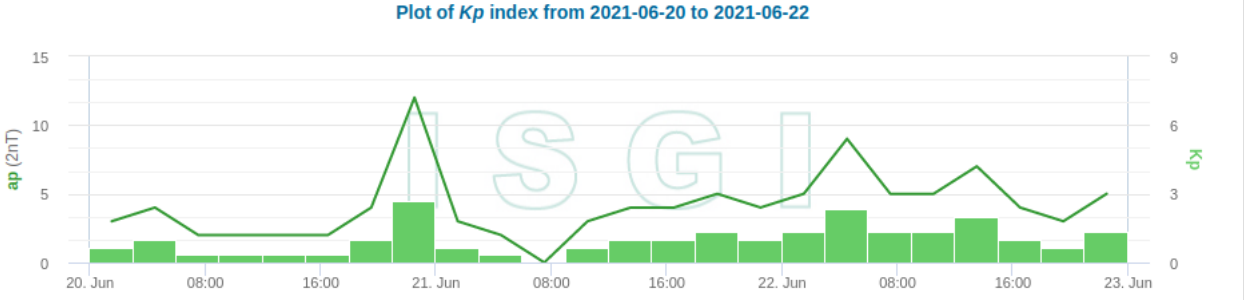

Figure 5.12: Kp index June (20-22), 2021

Table (5.1) shows the time of the eclipse day and its corresponding UT hours and the TEC in TEC Units (TECUs) for each begin, peak and end time of the eclipse for June 21 and the days before and after the eclipse day. For the purpose of reference the same time as the eclipse begin, peak and time were taken for the reference days.

Table 5.1: The time of eclipse (UT) for the eclipse day and the reference days and the corresponding TEC (TECU)

Time and Day		Djibouti(DJIG station)		Addis Ababa(ADIS station)	
Day	Time	UT hrs	TECU	UT hrs	TECU
June 19(Ref. day)	Begin	03:53	7.93	03:50	7.74
	Peak	05:03	10.3	04:57	13.46
	End	06:26	14.52	06:16	19.75
June 20(Ref. day)	Begin	03:53	6.56	03:50	6.52
	Peak	05:03	10.42	04:57	14.13
	End	06:26	14.69	06:16	20.5
June 21	Begin	03:53	6.56	03:50	7.32
	Peak	05:03	6.98	04:57	9.28
	End	06:26	10.88	06:16	15.05
June 22(Ref. day)	Begin	03:53	6.53	03:50	6.94
	Peak	05:03	8.66	04:57	12.3
	End	06:26	10.55	06:00	15.44
June 23(Ref. day)	Begin	03:53	7.6	03:50	7.99
	Peak	05:03	11.67	04:57	12.99
	End	06:26	16.04	06:16	19.9

Figures (5.13 - 5.15) show TEC measurements at ADIS Station for the days before, after and during the eclipse period. The coverage of the Sun was 89.13% and the eclipse magnitude over this region was 0.9187. The partial eclipse over Addis Ababa begins at around 06:50 EAT (03:50 UT), its maximum occurred at around 07:57 EAT (04:57 UT) and ends at about 09:16 EAT (06:16 UT).

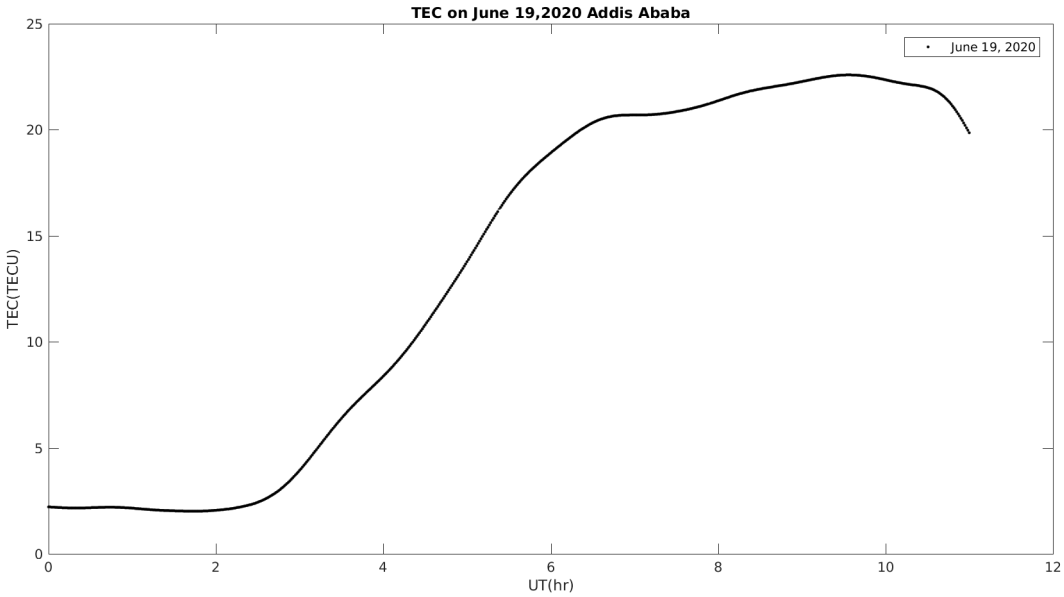

Figure 5.13: TEC over Addis Ababa, June 19, 2020

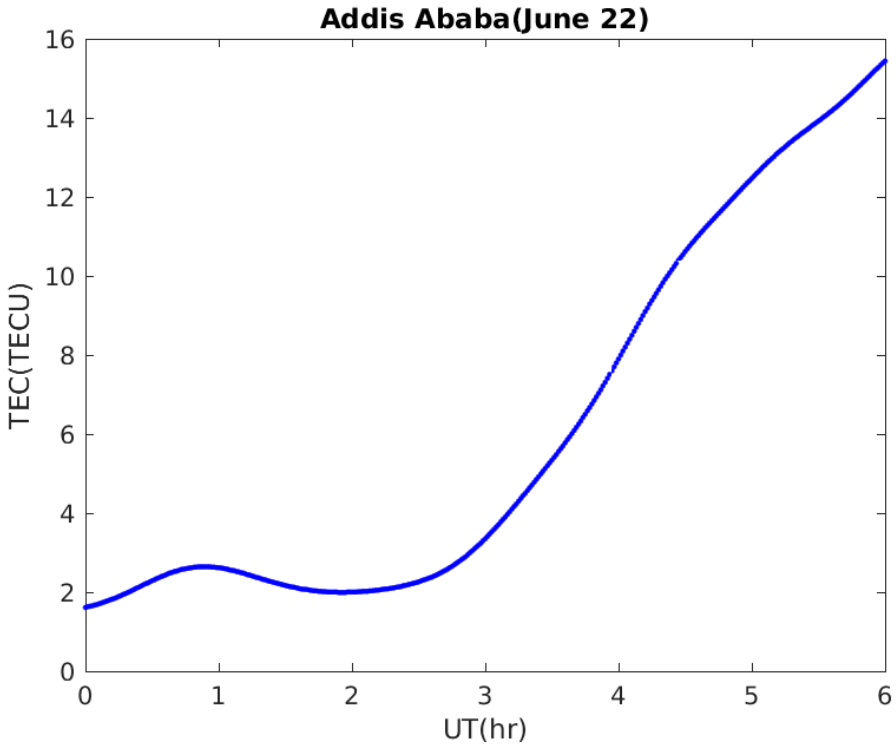

Figure 5.14: TEC over Addis Ababa, June 22, 2020

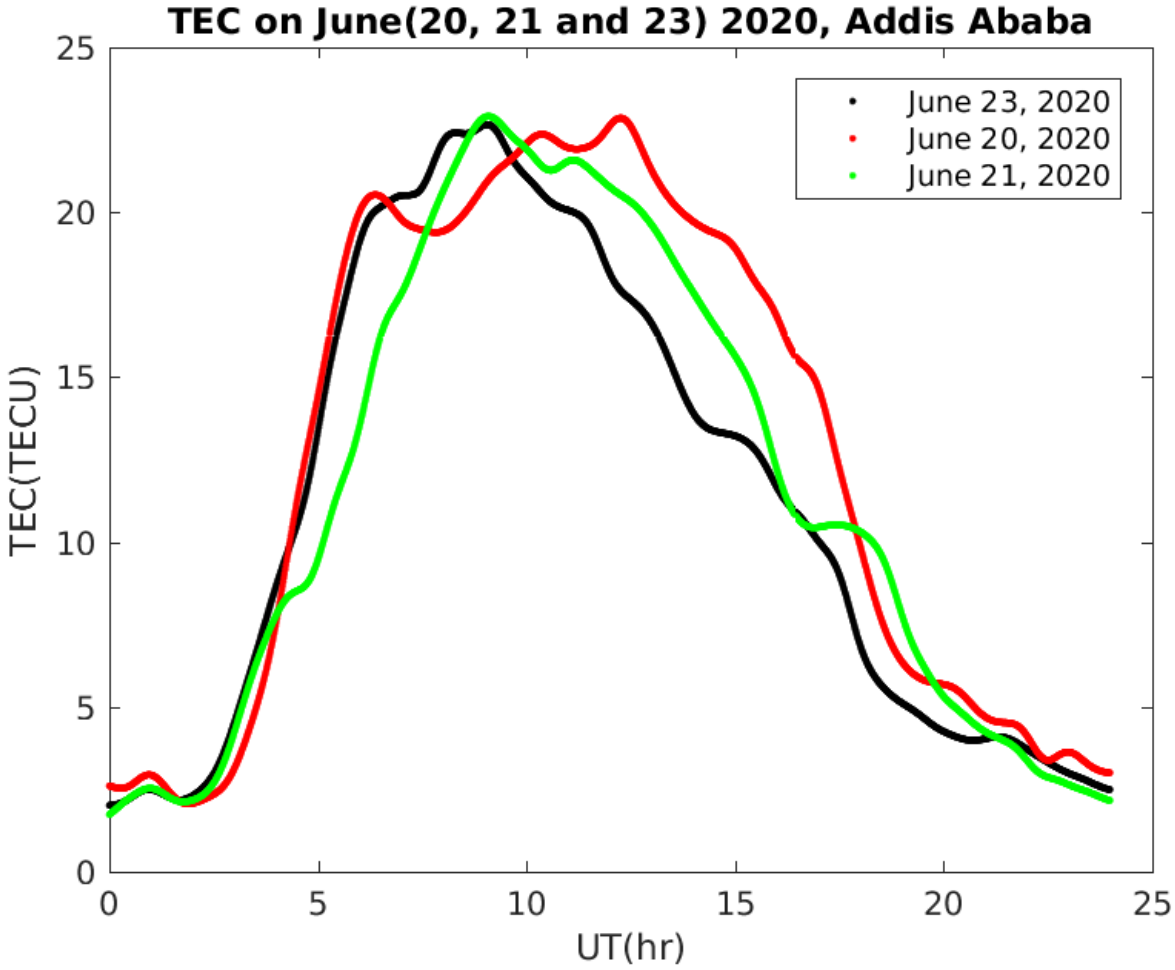

Figure 5.15: TEC over Addis Ababa, June (20, 21 and 23), 2020

The TEC depletion during the partial solar eclipse started at about 04:00 UT, about 10 minutes after the eclipse started. The TEC was decreased by about 4.85 TECU at the maximum eclipse and 5.45 TECU at the end of the eclipse compared to the day June 20. It was decreased by 4.18 TECU at the maximum eclipse and 4.7 TECU at the end of the eclipse compared to the day June 19. The data was not fully recorded after 06:00 UT over ADIS station, the day after the eclipse. The TEC was about 15.44 TECU at 06:00 UT. It was 20.03 TECU before the eclipse day at this same time and 13.53 TECU during the eclipse time. Therefore, the TEC was decreased by about 6.5 TECU compared to the day June 20 and 1.91 TECU compared to the day June 22 at 06:00 UT. It was decreased by 3.02 TECU at the maximum eclipse compared to the day June 22. It was decreased by 3.71 TECU at the maximum eclipse and 4.85 TECU at the end of the eclipse compared to the day June 23.

Table (5.2) shows the TEC of the three years (2010, 2011 and 2017) of June 21 and

the eclipse day.

Table 5.2: TEC on June 21 (2010, 2011, 2017 and 2020) Addis Ababa, ADIS station

Time(UT)	Years			
	2010	2011	2017	2020
03:50	10.42 TECU	8.62 TECU	8.27 TECU	7.32 TECU
04:57	16.8 TECU	16.11 TECU	14.35 TECU	9.28 TECU
06:16	20.55 TECU	22.44 TECU	20.13 TECU	15.05 TECU

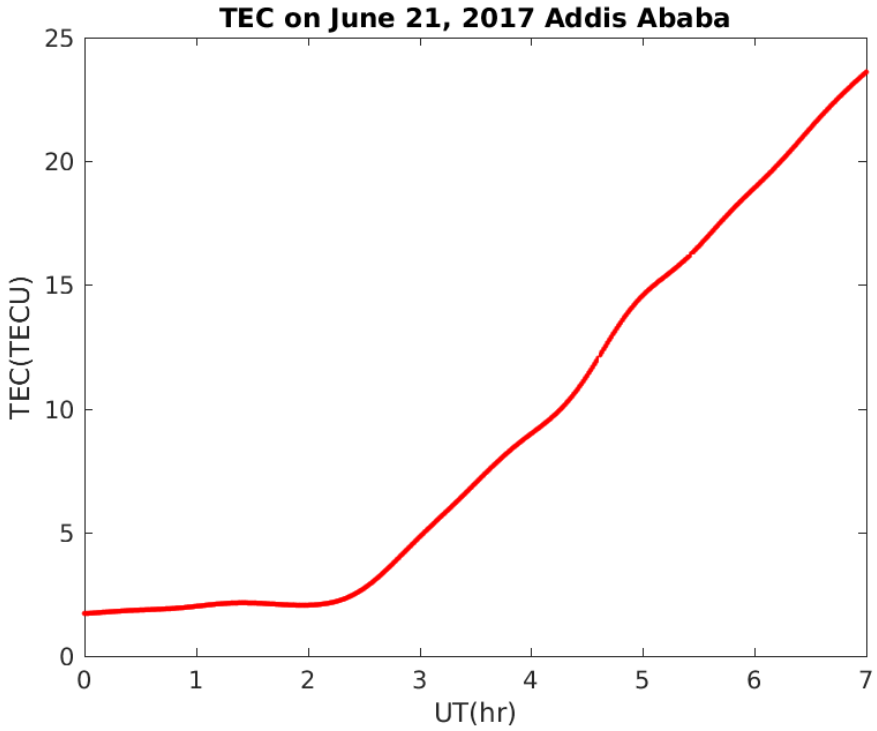

Figure 5.16: TEC over Addis Ababa, June 21, 2017

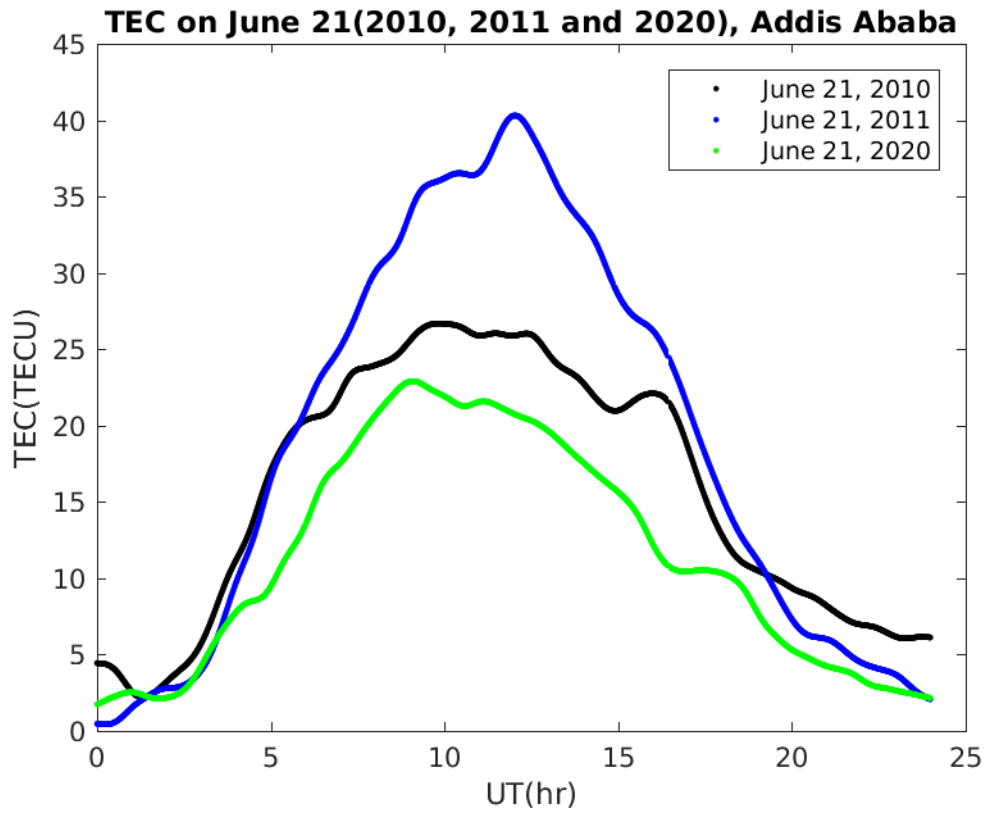

Figure 5.17: TEC over Addis Ababa, June 21 (2010, 2011 and 2020)

Figures (5.16 and 5.17) show TEC measurements on June 21 (2010, 2011, 2017 and 2020) for ADIS station. The TEC during the eclipse day was decreased by 7.52 and 5.50 TECU at peak and end time, respectively, compared to the year 2010. It was decreased by 6.83 and 7.39 TECU at peak and end time, respectively compared to the year 2011. It was decreased by 5.07 and 5.08 TECU at peak and end time, respectively, compared to the year 2017.

Figures (5.18 and 5.19) show TEC measurements over DJIG station, for the days before, after and during the eclipse period. The coverage of the Sun was 89.47% and the magnitude of the eclipse over this region was 0.9209. The partial solar eclipse over Djibouti begins at around 06:53 EAT (03:53 UT), its maximum occurred at about 08:03 EAT (05:03 UT) and the eclipse ends at about 09:26 EAT (06:26 UT).

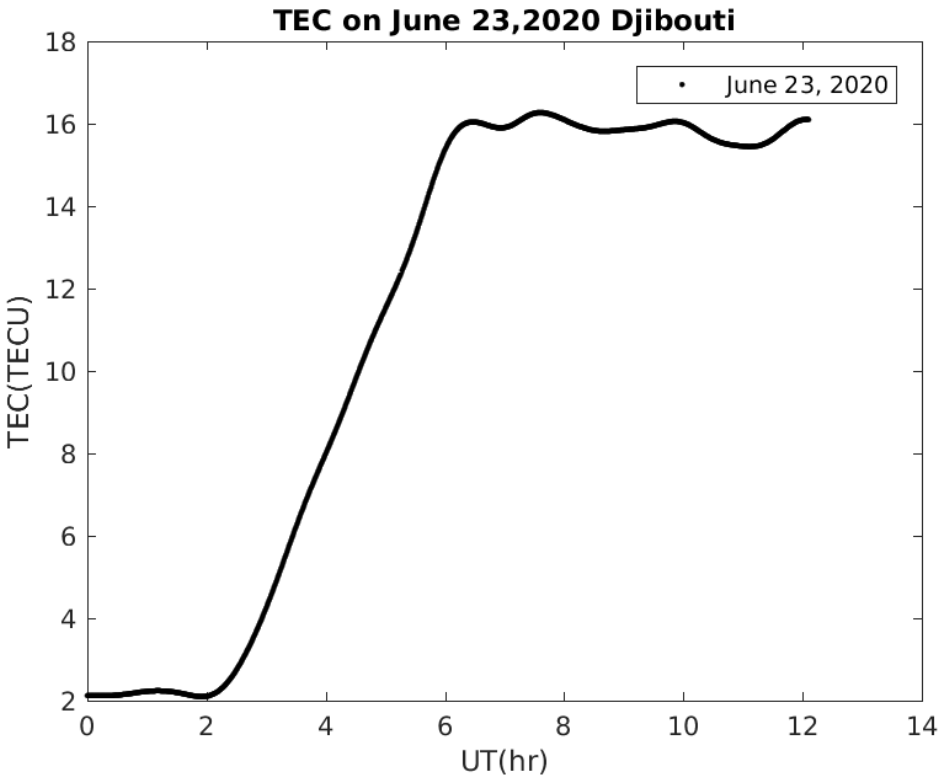

Figure 5.18: TEC over Djibouti, June 23, 2020

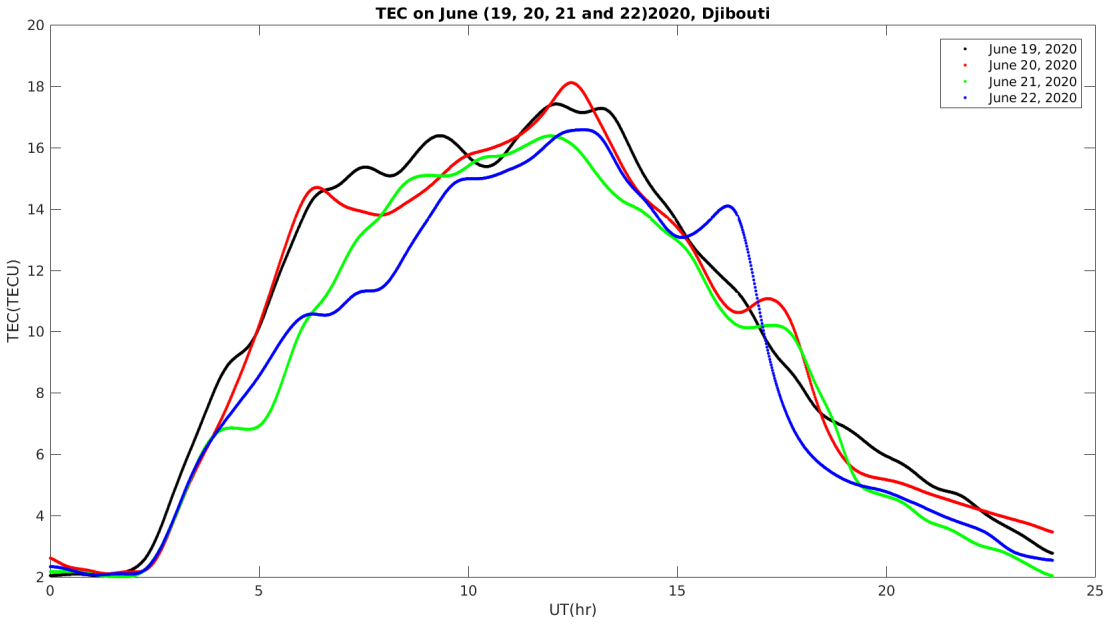

Figure 5.19: TEC over Djibouti, June(19, 20, 21 and 22),2020

No change in the TEC have been observed at the start time and continues the same until the depletion started at about 04:30 UT (37 minutes after the eclipse started).

The TEC was decreased by 3.32 TECU at the peak time and 3.64 TECU at the end of the eclipse time compared to the day June 19. At about 05:03 UT, which is the time of maximum, the TEC was decreased by about 3.52 TECU compared to the day June 20 and about 1.68 TECU compared to the day June 22. At 06:26 UT, which is the end time of the eclipse, the TEC was decreased by 3.81 TECU compared to the day June 20 and decreased by 0.33 TECU compared to the day June 22. It was decreased by 4.77 TECU at the maximum eclipse time and 5.16 TECU at the end of the eclipse time compared to the day June 23.

Table (5.3) shows the TEC of the three years (2017, 2018 and 2021) of June 21 and the eclipse day.

Table 5.3: TEC on June 21 (2017, 2018, 2021 and 2020) Djibouti, DJIG station

Time(UT)	Years			
	2017	2018	2021	2020
03:53	8.2 TECU	8.68 TECU	7.04 TECU	6.56 TECU
05:03	11.18 TECU	11.52 TECU	12.51 TECU	6.98 TECU
06:26	15.48 TECU	13.61 TECU	16.07 TECU	10.88 TECU

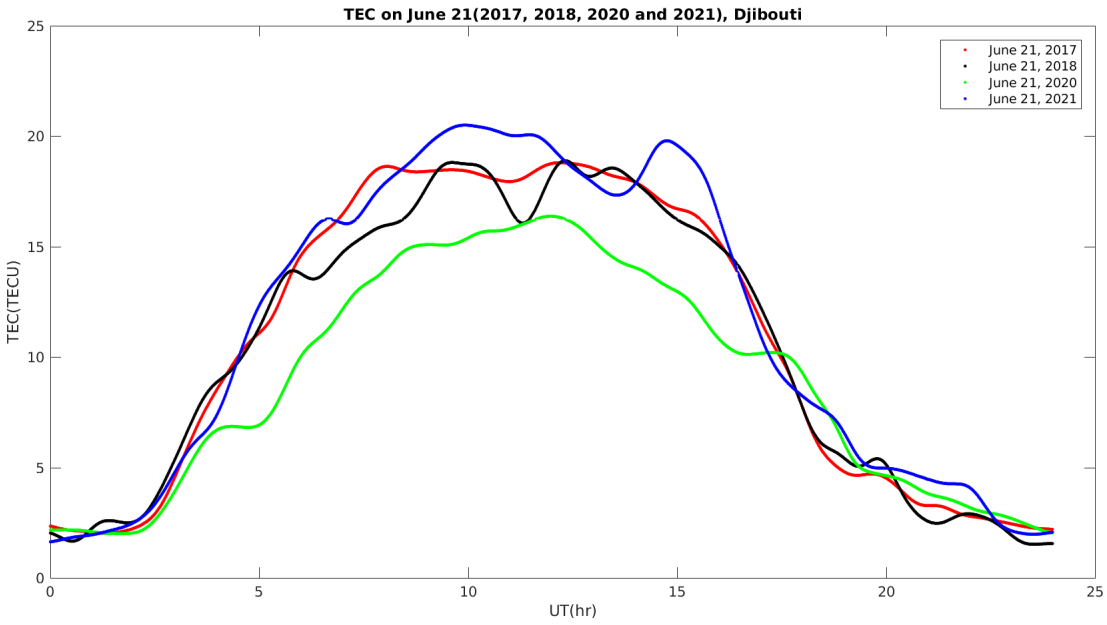

Figure 5.20: TEC over Djibouti, June 21 (2017,2018, 2020 and 2021)

Figure (5.20) show TEC measurements on 21 June, 2017, 2018, 2020 and 2021 for

DJIG station. The TEC during the eclipse day was decreased by 4.2 and 4.6 TECU at peak and end time, respectively compared to the year 2017. The TEC was decreased by 4.54 and 2.73 TECU at peak and end time, respectively compared to the year 2018. It was decreased by 5.53 and 5.19 TECU at peak and end time, respectively, compared to the year 2021.

A TEC depletion was observed a several minutes after the start time of the solar eclipse at both stations. 10 minutes after the eclipse over Addis Ababa and 37 minutes after the eclipse over Djibouti. At the start time of the partial eclipse, there was no change in the TEC. By taking the percentage TEC compared to a one day before (which have almost the same background TEC), a maximum depression of about 45 minutes after the maximum obscuration over ADIS and 15 minutes over DJIG was found. Researchers found a time lag between the maximum obscuration and the maximum TEC depletion. The ionosphere respond differently for the two stations, in which the start and lag time of ADIS was not the same as that of Djibouti. This could be because ADIS has a higher daily TEC than DJIG, and having more electrons and ions causes faster recombination. Because the loss rate is proportional to the the square of electron density [47].

As Cheng et al., [48] the time lag is because the topside ionosphere is less exposed to radiation and is impacted more by plasma redistribution, a delayed response is expected. For the same event, Aa et al., [49] studied nine stations for the morning, noon and dusk time eclipse and found a TEC reaching maximum depletion with approximately 30 minute time lag after maximum obscuration. Husin et al., [50] studied a solar eclipse on 9 March 2016 using two GNSS receivers [GISM and MNDO], and found a maximum reduction of 2–30 minutes after the maximum obscuration time and concluded these delays were related to photoionization and transport phenomena timescales. Solar eclipse of 20 March 2015 was studied by Stankov et al., over Belgium in the morning hours and by Hoque et al., over Europe [5, 8], they found a delay between the time of the maximum obscuration and the time of observed maximum TEC deviation of up to 40 minutes.

After the eclipse ended, the TEC began to return to normal levels, indicating that the observed deviations were caused by the partial solar eclipse [9, 51] and recovered fully after 1 hr over DJIG and 1 hr and 18 minutes over ADIS stations, compared to a one day before (which have almost the same background TEC). For the same

event, Huang et al., [6] found a TEC recovery near the end of the eclipse over 4 stations[LHAZ, HKWS, DJIG and GUAM] and Aa et al., [49] found a TEC gradually recovered to background level in 1 h after the eclipse ended. The recovery time for DJIG is faster than ADIS. It might be because of the eclipse duration, in which the duration is more in DJIG than ADIS. Because the ionosphere's state is directly related to ionizing solar radiation, a decrease in solar radiation due to the passage of the Moon's shadow is expected to result in a reduction of ionospheric electron density. However, depending on solar activity, season, local time and latitude, the ionospheric response to a single eclipse can vary greatly [52]. A maximum reduction of up to 35% were found in our study, in which the eclipse takes place in the morning hours. Huang et al., [6] suggested that the drop of TEC associated with the eclipse is significantly larger when it occurs around the noontime and Aa et al., [49] showed the maximum TEC reduction was approximately 30% for the dawn time eclipse and approximately 40–50% for the midday and afternoon eclipse.

The overall result in our study proved that the partial solar eclipse affects the photoionization. Since the ionosphere is mostly governed by the photoionization, the decrease in solar radiation consequently affects the density of the ionosphere. Djibouti and Addis Ababa are located at low latitudes, therefore, the TEC reduction might be further influenced by the eclipse's weakening of the fountain effect [7]. At low latitudes, dynamic activity associated with the equatorial anomaly have a considerable impact on the ionosphere, with transport mechanisms dominating photo chemical reactions [13]. As a result further research is needed in the low latitudes.

Chapter 6

Conclusion and Recommendations

6.1 Conclusion

During a solar eclipse, the Moon blocks solar radiation from reaching the ionosphere, which can have a significant impact on ionosphere variability. The ability to examine the effects of solar eclipse on the ionosphere has been made possible by the variability of TEC measured by dual frequency GPS receivers. The response of the ionospheric TEC to the June 21, 2020 annular solar eclipse was studied using two GPS stations found in Addis Ababa and Djibouti. The eclipse was partial over these two low latitude regions. To study ionospheric responses to the partial eclipse, the day of the eclipse, two days before, and two days after its occurrence and three years of June 21 GPS TEC measurements were analyzed for the purpose of comparison.

The effects of the partial solar eclipse that day were clearly seen on the ionospheric TEC at both stations. Both the GPS stations in Addis Ababa and Djibouti have detected a variation in ionospheric TEC over the region. It has been observed a TEC depletion a several minutes after the start time of the partial solar eclipse in both stations. At the start time of the partial eclipse, there was no change in the TEC and the depletion started 10 minutes after the eclipse started over ADIS station and 37 minutes over DJIG station. A high TEC depletion occurred 45 minutes and 15 minutes after the maximum obscuration over ADIS and DJIG stations, respectively. The ionosphere respond differently for the two stations, in which the start and lag time of ADIS was different than that of Djibouti. This might be because the daily TEC of ADIS is more than DJIG and having more electrons and ions lead to cause a faster recombination. The maximum deviation of TEC of up to 35% were observed compared

to the days before and after the eclipse.

After the eclipse ended, the TEC began to return to normal levels and recovered fully after 1 hr over DJIG and 1 hr and 18 minutes over ADIS stations, showing the partial solar eclipse affects the photoionization. Because the ionosphere is primarily formed by photoionization, a decrease in solar radiation has an impact on the ionosphere's density. DJIG has a faster recovery time than ADIS. It's possible that this is due to the eclipse duration, which is longer in DJIG. The results are consistent with previous studies for other eclipses by other researchers, such as [[47], [48], [49] [50], [5, 8]]. The findings of this study will provide insight into the types of changes that could occur at low geomagnetic and solar activities for future annular and partial solar eclipses in the morning hours in the low latitudes.

6.2 Recommendations

The major goal of this paper was to investigate the influence of a partial eclipse on TEC depletion using simply TEC data. However, because our study area is located at a low latitude, dynamic processes such as the equatorial ionization anomaly (EIA) have a significant impact on photoionization in this region. As a result, more research is needed in the low latitude and equatorial ionosphere regions, where TEC reduction may be influenced by dynamic activity. The annular solar eclipse of the June 21, 2020 crossed Lalibela, Alamata, Bahirdar and other Ethiopian regions. That day, GPS was not functioning and unable to collect any TEC data over those regions. Space-based satellites or other measurements can be used to study the behavior of the ionosphere over the regions during the annular solar eclipse for future studies.

Bibliography

[1] M. M. Alizadeh, H. Schuh, S. Zare, S. Sobhkhiz-Miandehi, and L.-C. Tsai, "Remote sensing ionospheric variations due to total solar eclipse, using gnss observations," *Geodesy and Geodynamics*, vol. 11, no. 3, pp. 202–210, 2020.

[2] S. K. Panda, S. S. Gedam, and G. Rajaram, "Gps derived ionospheric tec response to annular solar eclipse over indian region on 15 january 2010," in *2013 IEEE International Conference on Space Science and Communication (IconSpace)*, pp. 213–218, IEEE, 2013.

[3] F. Espenak, "Periodicity of lunar eclipses." `https://eclipse.gsfc.nasa.gov/LEsaros/LEperiodicity.html`, 2012.

[4] S. Jin, *Satellite Positioning: Methods, Models and Applications*. BoD–Books on Demand, 2015.

[5] S. M. Stankov, N. Bergeot, D. Berghmans, D. Bolsée, C. Bruyninx, J.-M. Chevalier, F. Clette, H. De Backer, J. De Keyser, E. D'Huys, *et al.*, "Multi-instrument observations of the solar eclipse on 20 march 2015 and its effects on the ionosphere over belgium and europe," *Journal of Space Weather and Space Climate*, vol. 7, p. A19, 2017.

[6] F. Huang, Q. Li, X. Shen, C. Xiong, R. Yan, S.-R. Zhang, W. Wang, E. Aa, J. Zhong, T. Dang, *et al.*, "Ionospheric responses at low latitudes to the annular solar eclipse on 21 june 2020," *Journal of Geophysical Research: Space Physics*, vol. 125, no. 10, p. e2020JA028483, 2020.

[7] W. Srigutomo, A. Singarimbun, W. Meutia, I. Djaja, B. Muslim, and P. Abadi, "Decrease of total electron content during the 9 march 2016 total solar eclipse

observed at low latitude stations, indonesia," *Annales Geophysicae Discussions*, pp. 1–12, 2019.

[8] M. M. Hoque, D. Wenzel, N. Jakowski, T. Gerzen, J. Berdermann, V. Wilken, M. Kriegel, H. Sato, C. Borries, and D. Minkwitz, "Ionospheric response over europe during the solar eclipse of march 20, 2015," *Journal of Space Weather and Space Climate*, vol. 6, p. A36, 2016.

[9] D. Okoh, A. Obafaye, M. Onudibia, and B. Rabiu, "Total electron content variations over abuja during the annular solar eclipse of september 1, 2016,"

[10] N. Ya'acob, M. Abdullah, and M. Ismail, "Gps total electron content (tec) prediction at ionosphere layer over the equatorial region," *Trends in Telecommunications Technologies*, 2010.

[11] E. Şentürk, M. A. Adil, and M. Saqib, "Ionospheric total electron content response to annular solar eclipse on june 21, 2020," *Advances in Space Research*, vol. 67, no. 6, pp. 1937–1947, 2021.

[12] C. Nayak, D. Tiwari, K. Emperumal, and A. Bhattacharyya, "The equatorial ionospheric response over tirunelveli to the 15 january 2010 annular solar eclipse: observations," in *Annales Geophysicae*, vol. 30, pp. 1371–1377, Copernicus GmbH, 2012.

[13] N. Jakowski, S. M. Stankov, V. Wilken, C. Borries, D. Altadill, J. Chum, D. Buresova, J. Boska, P. Sauli, F. Hruska, *et al.*, "Ionospheric behavior over europe during the solar eclipse of 3 october 2005," *Journal of Atmospheric and Solar-Terrestrial Physics*, vol. 70, no. 6, pp. 836–853, 2008.

[14] K. Mohanakumar, *Stratosphere troposphere interactions: an introduction*. Springer Science & Business Media, 2008.

[15] D. G. Andrews, *An introduction to atmospheric physics*. Cambridge University Press, 2010.

[16] J. Hughes, "Fundamentals of space physics,"

[17] Y. Kamide and A. C.-L. Chian, *Handbook of the solar-terrestrial environment*. Springer Science & Business Media, 2007.

[18] T. Immel, E. Sagawa, S. England, S. Henderson, M. Hagan, S. Mende, H. Frey, C. Swenson, and L. Paxton, "Control of equatorial ionospheric morphology by atmospheric tides," *Geophysical Research Letters*, vol. 33, no. 15, 2006.

[19] R. Bureau, "Handbook—the ionosphere and its effects on radiowave propagation," *International Telecommunication Union: Geneva, Switzerland*, 1998.

[20] R. Schunk and A. Nagy, *Ionospheres: physics, plasma physics, and chemistry*. Cambridge university press, 2009.

[21] H. Rishbeth and O. K. Garriott, "Introduction to ionospheric physics," *Introduction to ionospheric physics*, 1969.

[22] A. Komjathy, *Global ionospheric total electron content mapping using the Global Positioning System*. PhD thesis, University of New Brunswick Fredericton, 1997.

[23] Y. Memarzadeh, *Ionospheric modeling for precise GNSS applications*. Citeseer, 2009.

[24] B. Zolesi and L. R. Cander, *Ionospheric prediction and forecasting*. Springer, 2014.

[25] A. Hanslmeier, "The sun and space weather," in *Heliophysical Processes*, pp. 233–249, Springer, 2010.

[26] L. T. Elkins-Tanton, *The Earth and the Moon*. Infobase Publishing, 2006.

[27] I. C. Smith, "The what: A solar eclipse." `https://moonblink.info/Eclipse/what/solar`, 2019.

[28] D. Steel, *Eclipse. The celestial phenomenon that changed the course of history*. 2001.

[29] M. Mobberley, *Total solar eclipses and how to observe them*. Springer Science & Business Media, 2007.

[30] L. R. Cander, *Ionospheric space weather*. Springer, 2019.

[31] K. Yeh, D. Yu, K. Lin, C. Liu, C. Huang, W. Tsai, J. Liu, J. Xu, K. Igarashi, C. Xu, *et al.*, "Ionospheric response to a solar eclipse in the equatorial anomaly region," *Terrestrial, Atmospheric and Oceanic Sciences*, vol. 8, no. 2, pp. 165–178, 1997.

[32] S. Kumar and A. Singh, "Changes in total electron content (tec) during the annular solar eclipse of 15 january 2010," *Advances in space research*, vol. 49, no. 1, pp. 75–82, 2012.

[33] GPS.gov, "Other global navigation satellite systems (gnss)." `https://www.gps.gov/systems/gnss/`, 2020.

[34] GPS.gov, "The global positioning system." `https://www.gps.gov/systems/gps/`, 2021.

[35] M. L. El-Gizawy, *Development of an ionosphere monitoring technique using GPS measurements for high latitude GPS users*. Citeseer, 2003.

[36] G. Blewitt, "Basics of the gps technique: observation equations," *Geodetic applications of GPS*, pp. 10–54, 1997.

[37] V. Becerra and G. Esteban, "Analysis of stochastic properties of gps observables," tech. rep., Ohio State University. Division of Geodetic Science, 2008.

[38] C. Mekik and O. Can, "An investigation on multipath errors in real time kinematic gps method," *Scientific Research and Essays*, vol. 5, no. 16, pp. 2186–2200, 2010.

[39] H. Ebadi, "Positioning with gps," *KN Toosi University of Technology*, 2000.

[40] Y. A. Tariku, "Tec prediction performance of the iri-2012 model over ethiopia during the rising phase of solar cycle 24 (2009–2011)," *Earth, Planets and Space*, vol. 67, no. 1, pp. 1–10, 2015.

[41] A. G. Burrell, N. A. Bonito, and C. S. Carrano, "Total electron content processing from gps observations to facilitate ionospheric modeling," *GPS solutions*, vol. 13, no. 2, pp. 83–95, 2009.

[42] N. V. Rao, T. Madhu, and K. L. Kishore, "Geomagnetic storm effects on gps aided navigation over low latitude south indian region," *IJCSNS Int. J. Comput. Sci. Network Secur*, vol. 10, pp. 37–42, 2010.

[43] H. Tuna, O. Arikan, F. Arikan, T. L. Gulyaeva, and U. Sezen, "Online user-friendly slant total electron content computation from iri-plas: Iri-plas-stec," *Space weather*, vol. 12, no. 1, pp. 64–75, 2014.

[44] A. J. Mannucci, B. D. Wilson, and C. D. Edwards, "A new method for monitoring the earth's ionospheric total electron content using the gps global network," 1993.

[45] J. S. Shim, *Analysis of total electron content (TEC) variations in the low-and middle-latitude ionosphere*. Utah State University, 2009.

[46] G. Seemala and C. Valladares, "Statistics of total electron content depletions observed over the south american continent for the year 2008," *Radio Science*, vol. 46, no. 5, 2011.

[47] A. Brekke, *Physics of the upper polar atmosphere*. Springer Science & Business Media, 2012.

[48] K. Cheng, Y.-N. Huang, and S.-W. Chen, "Ionospheric effects of the solar eclipse of september 23, 1987, around the equatorial anomaly crest region," *Journal of Geophysical Research: Space Physics*, vol. 97, no. A1, pp. 103–111, 1992.

[49] E. Aa, S.-R. Zhang, H. Shen, S. Liu, and J. Li, "Local and conjugate ionospheric total electron content variation during the 21 june 2020 solar eclipse," *Advances in Space Research*, 2021.

[50] J. A Husin, S. Anggarani, S. Ekawati, and V. Dear, "Analysis of ionospheric irregularities during total solar eclipse 2016 based on gnss observation," in *Journal of Physics: Conference Series*, vol. 771, p. 012035, IOP Publishing, 2016.

[51] R. D. Didong and M. A. Momani, "The ionospheric response to the annular solar eclipse on 26 th january 2009," in *2009 International Conference on Space Science and Communication*, pp. 147–152, IEEE, 2009.

[52] A. J. Coster, L. Goncharenko, S.-R. Zhang, P. J. Erickson, W. Rideout, and J. Vierinen, "Gnss observations of ionospheric variations during the 21 august 2017 solar eclipse," *Geophysical Research Letters*, vol. 44, no. 24, pp. 12–041, 2017.

DECLARATION

This thesis has been submitted to Addis Ababa University department of physics as my original work, with the approval of my supervisor.

Name: Shibre Sete

Signature:————————-

This thesis has been submitted for examination with my approval as a student's advisor.

Name: Dr. Yitagesu Elfagd

Signature:————————

Place and date of submission:

Addis Ababa University

Department of Physics

October, 2021